

Rowan University

Rowan Digital Works

Theses and Dissertations

9-21-2022

EFFECTS OF CELL-CELL SIGNALING ON MESENCHYMAL STEM CELL MECHANOSENSING AND ADAPTATION TO DYNAMIC MATERIAL

Matthew E. Lowe
Rowan University

Follow this and additional works at: <https://rdw.rowan.edu/etd>



Part of the [Biomedical Engineering and Bioengineering Commons](#)

Recommended Citation

Lowe, Matthew E., "EFFECTS OF CELL-CELL SIGNALING ON MESENCHYMAL STEM CELL MECHANOSENSING AND ADAPTATION TO DYNAMIC MATERIAL" (2022). *Theses and Dissertations*. 3056.

<https://rdw.rowan.edu/etd/3056>

This Thesis is brought to you for free and open access by Rowan Digital Works. It has been accepted for inclusion in Theses and Dissertations by an authorized administrator of Rowan Digital Works. For more information, please contact graduateresearch@rowan.edu.

**EFFECTS OF CELL-CELL SIGNALING ON MESENCHYMAL STEM CELL
MECHANOSENSING AND ADAPTATION TO DYNAMIC MATERIALS**

by

Matthew E. Lowe

A Thesis

Submitted to the
Department of Biomedical Engineering
College of Engineering
In partial fulfillment of the requirement
For the degree of
Master of Science in Biomedical Engineering
at
Rowan University
September 1, 2022

Thesis Chair: Sebastián L. Vega, Ph.D., Assistant Professor, Department of Biomedical
Engineering

Committee Members:

Peter A. Galie, Ph.D., Associate Professor, Department of Biomedical Engineering
James M. Holaska, Ph.D., Associate Professor, Department of Biomedical Sciences

© 2022 Matthew E. Lowe

Dedications

I would like to dedicate this thesis to my mother, Monica M. Lowe and my father,
Peter W. Lowe.

Acknowledgements

I would like to express my appreciation to Doctor Sebastián Vega for his guidance and help throughout my research. The technical skills I have developed and the knowledge I have gained will prepare me well for future endeavors. I would like to thank Mohammed Mehdi Benmassaoud for his constant aid and mentorship during my undergraduate and graduate research. I would also like to thank Kirstene Gultian-Giddings for helping me synthesize polymers for my research and always being available to help me.

Finally, I would like to thank my family, specifically my mother, father, and brother, for their unwavering love and support in this process.

Abstract

Matt Lowe

EFFECTS OF CELL-CELL SIGNALING ON MESENCHYMAL STEM CELL
MECHANOSENSING AND ADAPTATION TO DYNAMIC MATERIALS

2021-2022

Sebastián L. Vega, Ph.D.

Master of Science in Biomedical Engineering

The goal of this research is to identify the role of engineered cell-cell signals on how cells sense material properties. Mesenchymal stem cells (MSCs) are adult cells whose behavior is regulated by matrix mechanosensing, which is characterized by stiffness-dependent changes in cell shape and the nuclear localization of mechanotransducer proteins including YAP (Yes-associated Protein). MSC area and nuclear YAP translocation increase with increasing stiffness, and although low levels of N-cadherin-based cell-cell signaling reduce this effect, two fundamental questions remain: (1) do engineered cell-cell signals at higher concentrations further reduce matrix mechanosensing, and (2) does N-cadherin signaling affect MSC adaptation to dynamic materials. To answer these questions, a stiffening hydrogel system was developed to independently control stiffness and HAVDI, a peptide that mimics cell-cell signaling. High concentrations of HAVDI (2 mM) reduce matrix mechanosensing on static hydrogels as seen by a decrease in area and nuclear YAP. The area of MSCs on soft HAVDI hydrogels that are stiffened does not change, but surprisingly nuclear YAP increases post-stiffening. These studies demonstrate that competing stiffness and cell-cell signals regulate matrix mechanosensing, and these insights are critical towards developing *in vitro* platforms to study ailments attributed to tissue stiffening including cancer, fibrosis, and aging.

Table of Contents

Abstract	v
List of Figures	x
Chapter 1: Introduction	1
1.1 Overview of Stem Cells	1
1.1.1 Overview of Mesenchymal Stem Cells.....	2
1.1.2 Effect of External Factors on Stem Cell Behavior.....	3
1.2 Cellular Matrix Mechanosensing.....	3
1.2.1 Mechanism Behind Cellular Matrix Mechanosensing.....	3
1.2.2 Mechanical Memory	5
1.2.3 Mechanoadaptation	6
1.2.4 Limitations of Current MSC Expansion Techniques.....	7
1.3 Biomaterials	8
1.3.1 Metals and Ceramics.....	8
1.3.2 Hydrogels.....	10
1.4 Effect of Substrate Stiffness on MSC Behavior	11
1.4.1 Role of Stiffness on 2-Dimensional Hydrogels	11
1.4.2 Role of Stiffness in 3-Dimensional Hydrogels	11
1.5 Effect of Cell-Cell Signaling on MSC Behavior	12
1.5.1 Physiological Importance of Cell-Cell Signaling	12
1.5.2 Mechanism Behind Cell-Cell Signaling	13

Table of Contents (Continued)

1.5.3 Identification of N-Cadherin Mimetic Peptide	14
1.6 Central Hypothesis	14
Chapter 2: Creating Dynamic Hydrogel Systems Using Multiple Macromers	19
2.1 Introduction.....	19
2.1.1 Establishing a Dynamic Hydrogel System	19
2.1.2 Methacrylated Hyaluronic Acid	20
2.1.3 Norbornene-Modified Hyaluronic Acid	21
2.2 Materials and Methods.....	22
2.2.1 MeHA Synthesis	22
2.2.2 MeHA Hydrogel Formation.....	23
2.2.3 NorHA Synthesis	24
2.2.4 NorHA Hydrogel Formation.....	25
2.2.5 Scrambled HAVDI Synthesis	26
2.2.6 Mechanical Testing of Hydrogels	27
2.3 Results and Discussion	27
2.3.1 H-NMR Analysis of MeHA.....	27
2.3.2 Mechanical Characterization of MeHA.....	29
2.3.3 H-NMR Analysis of NorHA	31
2.3.4 Mechanical Characterization of NorHA	32
2.3.5 MALDI Analysis of Scrambled HAVDI.....	34
Chapter 3: MeHA Hydrogels to Evaluate the Effect of HAVDI on MSCs	36

Table of Contents (Continued)

3.1 Overview.....	36
3.2 Materials and Methods.....	36
3.2.1 MSC Culture	36
3.2.2 MSC Staining.....	37
3.2.3 Imaging and Analysis	38
3.2.4 Statistical Analysis.....	38
3.3 Results and Discussion	39
3.3.1 Static MSC Area Analysis on MeHA	39
3.3.2 Static MSC Morphology Analysis on MeHA.....	41
3.3.3 Static MSC Nuclear YAP Analysis on MeHA	44
3.3.4 Dynamic MSC Area Analysis on MeHA.....	46
3.3.5 Dynamic MSC Morphology Analysis on MeHA	48
3.3.6 Dynamic MSC Nuclear YAP Analysis on MeHA.....	51
3.4 Conclusion	52
Chapter 4: NorHA Hydrogel to Evaluate Varying HAVDI Concentrations on MSCs	55
4.1 Overview.....	55
4.2 Materials and Methods.....	55
4.2.1 MSC Culture	55
4.2.2 MSC Staining.....	56
4.2.3 Imaging and Analysis	57
4.2.4 Statistical Analysis.....	58

Table of Contents (Continued)

4.3 Results and Discussion	58
4.3.1 Static MSC Area Analysis on NorHA	58
4.3.2 Static MSC Morphology Analysis on NorHA.....	60
4.3.3 Static MSC Nuclear YAP Analysis on NorHA	64
4.3.4 Dynamic MSC Area Analysis on NorHA.....	65
4.3.5 Dynamic MSC Morphology Analysis on NorHA	66
4.3.6 Dynamic MSC Nuclear YAP Analysis on NorHA.....	68
4.4 Conclusion	70
Chapter 5: Summary and Future Directions	72
5.1 Summary	72
5.2 Effect of Mechanical Dosing on MSCs	73
5.2.1 NorHA Hydrogel System to Evaluate the Effect of Mechanical Dosing	74
5.2.2 Preliminary Results	74
5.3 Effect of Engineered Cell-Cell Signaling on MSC Remodeling in 3D	76
5.3.1 MSC Behavior Encapsulated within 3D Hydrogels	76
5.3.2 Theoretical Effect of Cell-Cell Signaling on MSC Matrix Remodeling	77
References.....	79

List of Figures

Figure	Page
Figure 1. Overview of MeHA Synthesis Procedure	23
Figure 2. Peptide Coupling to MeHA and Soft MeHA Hydrogel Formation	24
Figure 3. Overview of NorHA Synthesis Process	25
Figure 4. Overview of the Soft NorHA Hydrogel Formation Process	26
Figure 5. H-NMR Analysis of MeHA	29
Figure 6. Mechanical Characterization of MeHA Hydrogels	31
Figure 7. H-NMR Analysis of NorHA	32
Figure 8. Mechanical Characterization of NorHA Hydrogels	34
Figure 9. MALDI Analysis of the Scrambled HAVDI Peptide.....	35
Figure 10. Cellular and Nuclear Area of MSCs on Static MeHA Hydrogels.....	40
Figure 11. Cellular and Nuclear Morphology of MSCs on Static MeHA Hydrogels	44
Figure 12. Nuclear YAP of MSCs Cultured on Static MeHA Hydrogels	46
Figure 13. Cellular and Nuclear Area of MSCs on Dynamic MeHA Hydrogels	48
Figure 14. Cellular and Nuclear Morphology of MSCs on Dynamic MeHA Hydrogels	50
Figure 15. Nuclear YAP of MSCs Cultured on Dynamic MeHA Hydrogels.....	52
Figure 16. Cellular and Nuclear Area of MSCs on Static NorHA Hydrogels.....	60
Figure 17. Cellular and Nuclear Circularity of MSCs on Static NorHA Hydrogels	62
Figure 18. Cellular and Nuclear Aspect Ratio of MSCs on Static NorHA Hydrogels.....	63
Figure 19. Nuclear YAP of MSCs Cultured on Static NorHA Hydrogels	65
Figure 20. Cellular and Nuclear Area of MSCs on Dynamic NorHA Hydrogels	66

List of Figures (Continued)

Figure	Page
Figure 21. Cellular and Nuclear Morphology of MSCs on Dynamic NorHA Hydrogels.....	68
Figure 22. Nuclear YAP of MSCs Cultured on Dynamic NorHA Hydrogels.....	69
Figure 23. Flow Cytometry of High and Low Passage MSCs.....	76

Chapter 1

Introduction

1.1 Overview of Stem Cells

Stem cells are unspecialized cells found throughout the body that have two unique features: self-renewal and differentiation [1]. Self-renewal allows a stem cell to make exact an exact copy of itself. Differentiation is the process by which a stem cell transforms into a specialized cell with a specific function [2]. These properties make stem cells very promising for use in regenerative medicine, therapeutics, and disease modeling.

There are three main classes of stem cells: pluripotent stem cells (PSC), induced pluripotent stem cells (iPSC), and multipotent stem cells. PSCs have the greatest range of differentiation capabilities as they can give rise to most cell types. While the therapeutic potential of PSCs is great, there are challenges sourcing these cells because they are derived from embryos [3]. Similar to PSCs, iPSCs also have the ability to differentiate into most cell types. iPSCs are different from PSCs in that iPSCs are derived from any specialized cell type that has been treated with certain factors that revert the cell to a pluripotent state. While iPSCs overcome the challenge of cell sourcing, they are not without limitations. One prominent issue with iPSCs is the potential to develop into tumors [4]. Multipotent stem cells have a more limited differentiation capacity than PSCs and iPSCs. Despite this limitation, they are commonly used in research as they can be sourced from various locations throughout the body, making them relatively easy to obtain [5]. All stem cells have unique advantages and disadvantages, but there are also

shared challenges facing large scale use of stem cells as therapeutic agents. Long-term storage and cellular manufacturing are two of the greatest limitations on widespread use of stem cell therapies [6]. Overcoming these obstacles would improve the clinical success of stem cell therapies.

1.1.1 Overview of Mesenchymal Stem Cells

Mesenchymal stem cells (MSC) are a specific type of adult stem cell that can differentiate into cells that comprise skeletal and connective tissues. To classify a cell as an MSC, it must meet three criteria: (1) it must attach to tissue culture plastic (TCP) under typical expansion conditions; (2) it must express surface markers CD105, CD73, and CD90 and not express markers CD45, CD34, CD14 or CD11 β , CD79 α ; (3) it must possess the ability to differentiate into osteoblasts, chondrocytes, and adipocytes when cultured in vitro [7]. There are many sources of MSCs in the body, with bone marrow, adipose tissue, and dental pulp being among the most common [1, 8]. Although all MSCs display the same criteria, there are differences observed among sourcing locations. For example, MSCs isolated from bone marrow preferentially differentiate into osteoblasts and chondrocytes while adipose-derived MSCs favor adipogenic differentiation [9]. Additionally, MSCs sourced from the same location display variability among donors, specifically regarding metabolic rate, cell morphology, and alignment [10]. Despite the broad impact that MSCs can have in regenerative medicine, there is a need to improve population homogeneity in culture conditions.

1.1.2 Effects of External Factors on Stem Cell Behavior

Stem cell behavior can be easily manipulated by a wide range of mechanical and biochemical stimuli due to their undifferentiated nature. Mechanical cues, such as substrate stiffness, dimensionality, and degradability have all shown to influence stem cell properties [11-13]. Biomaterial elastic modulus has shown potential to alter differentiation, morphology, and proliferation of stem cells [13-15]. Cell-cell and cell-matrix interactions are the driving forces behind microenvironment control over stem cell behavior. Stem cell properties including proliferation, differentiation, and migration are all affected by various external factors. Physical cues, such as substrate stiffness, topography, stress relaxation, shear stress, dimensionality, and cell-cell contact all impact stem cells behavior [11, 13, 16-18]. Additionally, chemical factors including growth factors and secreted cytokines have a significant impact on stem cell behavior [19, 20]. While this property allows stem cells to have a wide range of potential uses, it also provides challenges with controlling desired outcomes.

1.2 Cellular Matrix Mechanosensing

1.2.1 Mechanism Behind Cellular Matrix Mechanosensing.

Cells in vivo are naturally surrounded by the extracellular matrix (ECM), which is comprised of many proteins and presents a variety of ligands and mechanical properties to the cell. Receptor-ligand interactions and physical properties of the surrounding matrix have shown to affect cell behavior [21-23]. For physical properties of the surrounding matrix to impact MSC behavior, cells must be able to interpret mechanical information. Matrix mechanosensing is the process by which cells interact with their surroundings by

transforming mechanical stimuli into chemical signaling. Focal adhesions are the primary structure responsible for cellular matrix mechanosensing [24]. Focal adhesions are made up of several proteins working in unison, with integrins being an important family of proteins [25]. Integrins are transmembrane receptor proteins that interact with proteins in the ECM. Integrins are unique in that they are bidirectional signaling proteins, meaning that they can attach to ligands outside of the cell or interact with signaling molecules within the cytoplasm [26]. Other proteins groups within focal adhesions include actin-linking proteins, such as talin and vinculin, actin polymerizing proteins, such as zyxin and formins, and signaling proteins, such as focal adhesion kinase. The entire focal adhesion complex is mechanoresponsive and mechanosensitive, meaning that each component feeds into a loop that both modulates and is modulated by signaling molecules [25].

The proteins that make up the focal adhesion complex are influenced by intracellular forces such as actin polymerization and myosin contractility and extracellular forces, such as matrix elastic modulus [24]. Increased cellular tension facilitates more focal adhesion assembly to further mechanosense ECM stiffness. The forces generated by the actin cytoskeleton are impacted by cell-matrix interactions [25]. The interactions between integrins and the surrounding matrix trigger focal adhesion kinase signaling, which results in the stimulation of small G proteins, such as Rho and Rac. Rho causes a Rho kinase (ROCK) signaling cascade, which increases cytoskeletal tension via the phosphorylation of myosin light chain [27]. When cells experience increased cytoskeletal tension and Rho is activated, the transcriptional regulator, YAP (Yes-associated Protein)

is relocated to the nucleus [28]. Certain cellular behaviors are associated with nuclear YAP, such as a large, spread morphology, increased number of focal adhesions, an osteogenic differentiation. Conversely, MSCs with cytosolic YAP have a small, round morphology, fewer focal adhesions, and favor adipogenic differentiation [11, 28, 29]. The localization of YAP is an effective measure of how a cell is mechanosensing its surroundings.

1.2.2 Mechanical Memory

It has been well documented that substrate stiffness plays a key role in altering MSC gene expression [11, 30-32]. However, the role of substrate stiffness extends beyond a cell's current cell-ECM interactions. Yang et al. has demonstrated that cells possess an ability termed mechanical memory, in which the cellular behaviors driven by previous mechanical environments persist when the matrix mechanics change. The effects of mechanical memory have drastic implications on cell culture, specifically in vitro cellular expansion. Currently, most cells are expanded on tissue culture plastic (TCP), which is orders of magnitude stiffer than the elastic moduli range of native tissues [33]. When MSCs were cultured on TCP for short periods of time before being transferred to soft hydrogels, YAP was able to localize in the cytoplasm. However, as cells were dosed on TCP for longer periods of time, nuclear YAP localization significantly increased, even when the cells were transferred to a soft hydrogel [33]. Increased passaging has already proven to decrease the differentiation capability of MSCs, and the mechanical memory from numerous TCP expansions could be a contributing factor [34]. These results create a need for a better cell culture platform that promotes cell growth and proliferation without

significantly influencing cell behavior. While creating a unique culture system that is more effective than TCP expansion is beyond the scope of this dissertation work, the combinatorial effect of mechanical and biochemical stimuli on MSC behavior will be explored.

1.2.3 Mechanoadaptation

While MSCs are influenced by the mechanical information about previous substrates, they are also capable of adapting to new mechanical environments. Mechanoadaptation is the counterpart to mechanical memory. When MSCs are transferred to soft substrates after being expanded on TCP for a brief period, most cells adapt to the soft substrate. However, as the length of mechanical dosing time on TCP increases, fewer MSCs will mechanoadapt to the soft substrate [33]. The gradual decrease in cellular mechanoadaptation that corresponds with increased TCP expansion time suggests that MSC populations may begin to express heterogenous behaviors that can skew fundamental insights on cell-material interactions and severely limit the large-scale manufacturing of cells for cellular therapies. The relationship between mechanical memory and mechanoadaptation is intertwined. When cells retain much information about their previous mechanical environment (e.g., stiff TCP expansion dishes), fewer cells will adapt to new biomaterials (e.g., soft 3D hydrogels with signals that guide MSC cartilage differentiation). One effective method of studying mechanoadaptation in vitro is through dynamic hydrogel systems. Yang et al. used a hydrogel system that could be softened on demand using a photocleavable crosslinker. The results showed that short mechanical dosing on TCP was fully reversible with sufficient time on a softened

hydrogel, by examining nuclear YAP. However, as the length of dosing time increased, nuclear YAP was unable to return to baseline soft levels, and eventually, there was a complete loss in mechanoadaptation [33]. These results reinforce the idea that MSCs can adapt to new substrates, and this is contingent on mechanical memories accrued from previous culture environments. A separate study by Guvendiren and Burdick used a stiffening hydrogel system to evaluate MSC behavior. These results examined cellular morphology and traction force to demonstrate that most MSCs were able to adapt to stiff substrates when mechanical dosing and mechanoadaptation durations were short. When MSCs were dosed on soft hydrogels for a short duration and given a long duration to adapt to the stiffened hydrogel, almost all cells adapted and displayed behavior associated with the stiff hydrogel. Conversely, when dosing and adaptation times were longer but equal, a heterogeneous population of cells was achieved [35]. This further suggests that mechanoadaptation is dependent on the mechanical memory of the cells. The combined results from both studies illustrate the importance of mechanical memory and mechanoadaptation on MSC behavior. Prolonged periods of mechanical dosing can lead to unintended consequences that influence cells at later times. Exploring how the upstream signals of matrix mechanosensing during mechanical dosing are influenced by other biochemical interactions, such as cell-cell signaling, could help improve cell expansion techniques at small and large scales.

1.2.4 Limitations of Current MSC Expansion Techniques

MSCs harvested from adult tissues (e.g., bone marrow, adipose tissue) must be separated from other cell types, and the resulting number of MSCs is low [36]. In order to

attain the cell counts required for experimental and clinical use, MSCs need to divide while maintaining their native properties. Typically, expansion occurs on TCP, which has an elastic modulus ~ 3 GPa. This material has a stiffness that is orders of magnitude greater than the elastic modulus of native tissues [15]. Due to mechanical memory, MSCs can store mechanical information which influences downstream signaling and stem cell behavior. Expanding MSCs on supraphysiological stiff TCP creates mechanical biases that drive MSCs towards phenotypes associated with high stiffness environments, even if the cells are transferred to softer materials post-expansion [33]. TCP expansion also leads to the formation of heterogenous MSC populations, which are detrimental to large-scale cell manufacturing initiatives.

1.3 Biomaterials

1.3.1 Metals and Ceramics

Biomaterials can be classified as any object used alongside a living organism to guide the trajectory of a remedial procedure or medical device [37]. There are countless substances that can be used to make a biomaterial, each with unique properties and advantages that can be tailored to perform a given task. Biomaterials can be classified in numerous ways, including the type of substance that comprises the biomaterial, how the material associates with living organisms, or if the material is found in nature or created by humans [38]. There are three general substances that make up most biomaterials: metals, ceramics, and polymers. The substance that makes up a biomaterial must be carefully chosen to meet the needs intended for the biomaterial to fulfill.

Metals offer a wide range of benefits, such as high mechanical stability, strong load bearing properties, and excellent electrical conductivity. Metals are often mixed with other chemical elements to create alloys with improved properties over the metal itself [39]. The main disadvantage of metal biomaterials is that the material can degrade over time and produce debris that is toxic to the body [40].

Ceramic materials on the other hand generally have high biocompatibility, low degradability, and do not corrode. Ceramics can be further broken down into three subclasses: bioinert, bioactive, and bioresorbable [41]. Bioinert ceramics have little interaction with surrounding tissue and are often used for bone and dental repair [42]. Bioactive ceramics are able to interact with bone tissue and improve the corrosion resistance properties of the ceramic, making it ideal for bone tissue engineering [41]. Bioresorbable ceramics degrade over time and are slowly supplanted by new bone tissue. The degradability of bioresorbable ceramics facilitates its use in treating bone defects and fractures without generating a large immune response [43]. Ceramic biomaterials may be limited by their brittle nature, meaning that they have little plastic deformation and will shatter rather than deform [44].

Polymers are natural or synthetic materials made from a series of long, repeating subunits called monomers [45]. Polymers can be highly modified to create a wide range of materials that can be tuned to meet specific needs. One property that is important for most biomaterials is biocompatibility of the material and any components of the material that may be created during its degradation. Other properties, such as controlled

degradation rate, mechanical properties that mimic the target tissue, cell adhesion, and electrical conductivity, can be tailored to achieve desired tasks [46].

1.3.2 Hydrogels

Hydrogels are a soft class of biomaterials that consists of highly hydrated crosslinked polymer chains [47]. Hydrogels can be formed with natural, synthetic, or composite polymers, providing a broad range of properties and applications. There are several ways that hydrogels can be crosslinked, including self-assembly [48], physical entanglement [49], and chemical crosslinking [50]. The method of hydrogel crosslinking may depend on the given application. For instance, self-assembling hydrogels are ideal to inject for in vivo applications because they do not require surgical insertion, and do not require an external stimulus to trigger gelation. When a higher elastic modulus is desired, other crosslinking methods, such as chemical crosslinking may be preferred. Typically, hydrogels have a relatively low elastic modulus compared to other polymeric biomaterials including metals and ceramics, due to their high water content [51]. However, a combination of multiple crosslinking methods can be utilized to increase the elastic modulus. Additionally, the chemical properties of hydrogels can be tuned by functionalizing bioactive peptides to the hydrogel polymer backbone [52]. The wide range of material properties and peptide coupling ability make hydrogels particularly useful for studying specific cell-matrix interactions.

1.4 Effect of Substrate Stiffness on MSC Behavior

1.4.1 Role of Stiffness on 2-Dimensional Hydrogels

The effect of biomaterial stiffness on MSC behavior has been well documented, with results varying across dimensionality (2D vs. 3D). When the matrix surrounding a cell is stiffened, focal adhesions can sense this change. When MSCs are cultured atop 2-dimensional substrates, the elastic modulus of the material heavily influences MSC behavior. Soft substrates inhibit cell contractility, leading to a small, round morphology [11]. Additionally, soft substrates result in cytoplasmic localization of YAP. YAP is an important gene regulator within MSCs and alters many behaviors including proliferation, differentiation, and matrix mechanosensing. Conversely, biomaterials with a high stiffness increase lead to greater cell contractility a large, spread morphology, and nuclear localization of YAP [13].

1.4.2 Role of Stiffness in 3-Dimensional Hydrogels

In 3-dimensional substrates, MSC phenotype is altered by the elastic modulus of the material as well as the degradability of the crosslinker. When MSCs are encapsulated in a hydrogel with degradable crosslinks, cellular volume increases at intermediate (~5 kPa) stiffnesses and decreases at high (~20 kPa) and low (~1 kPa) stiffnesses. Despite causing a decrease in overall cell volume, low stiffness hydrogels result in the greatest amount of MSC spreading. As the stiffness increases, MSCs display a more rounded morphology. Hydrogels with non-degradable crosslinker guide MSCs towards a small volume and a round morphology [11]. For MSCs to spread within a 3-Dimensional substrate, they must be able to break down and remodel the surrounding environment. This explains why

encapsulated MSCs display a spread morphology within low stiffness hydrogels, because there are fewer crosslinks to degrade. MSCs display a small, round morphology and preferentially differentiate into adipose cells. This behavior is driven by a low mechanical activity of the cells and relocation of YAP to the cytoplasm [11].

1.5 Effect of Cell-Cell Signaling on MSC Behavior

1.5.1 Physiological Importance of Cell-Cell Signaling

As previously discussed, cells possess the ability to transduce mechanical stimuli into chemical information that affects their behavior. In addition to interpreting ECM mechanics, interactions between cells can also influence MSC behavior. Integrins play a role in cell-cell attachment, much like they facilitate cell-ECM attachment for matrix mechanosensing. However, the key proteins that regulate cell-cell interactions are cadherins. Cadherins are transmembrane proteins that form adherens junctions with cadherin proteins on other cells [53]. Cadherins are linked to the actin cytoskeleton by catenin proteins, which are essential to the adherens junction function [54]. The ability for cells to effectively communicate with each other is crucial for biological functions, such as development and maintaining homeostasis [55]. During development of mesenchymal tissues, much of the mechanical stimuli are derived from adherens junctions because there are more cells than matrix present. Over time, cell-cell binding decreases as cells differentiate and associate with the surrounding ECM that is being deposited. As such, cadherin binding decreases. Due to the interplay between cell-cell and cell-ECM interactions, this suggests that cell-cell signaling plays an important role in guiding development [22]. In addition to shaping the development of mesenchymal

tissue, cell-cell signaling plays a vital role in maintaining homeostasis. Within muscle tissue, cadherin proteins link muscle stem cells to myofibers under normal conditions, forming adherens junctions. However, when muscle tissue needs to be replaced, cadherins begin forming connections with other stem cells, signaling them to differentiate and repair the damaged tissue [56]. Dysfunction related to cell-cell signaling can have detrimental effects, such as promotion of cancer growth [57, 58]. By studying the effects of cell-cell signaling, a greater understanding of these mechanisms can be achieved.

1.5.2 Mechanism Behind Cell-Cell Signaling

For cells to communicate with one another, there must be a chemical process that causes cell-cell signaling to affect cell behavior. While there are many downstream signaling pathways that are affected by cell-cell signaling, many of which are not fully understood, the Hippo pathway has proven to be triggered by interactions between cells [59]. Activation of the Hippo pathway can be triggered by numerous cellular mechanisms, with one such path being adherens junctions, specifically the interactions between cadherin and catenin proteins. The Hippo pathway is made up of a series of interactions between serine kinases and proteins that influence a transcription regulator to alter gene expression that affects cell size and morphology. The signaling cascade occurs via a series of protein activations that ultimately lead to the phosphorylation of transcriptional coactivators YAP and TAZ (Transcriptional coactivator with PDZ-binding motif) by Lats proteins. Phosphorylated YAP/TAZ is precluded from the nucleus and forced to remain in the cytoplasm. The purpose of YAP is to collaborate with TEAD transcription factors inside the nucleus, which activates genes that promote cellular

growth and prevent apoptosis. Therefore, the Hippo pathway serves to limit cellular growth and allow programmed cellular death by excluding YAP/TAZ from the nucleus [60]. However, the cell-cell binding at adherens junctions is merely a trigger to activate the Hippo pathway and phosphorylate YAP. Disrupting elements of the Hippo pathway, such as knocking down catenin or blocking the signaling cascade, results in greater nuclear YAP and promotes cellular growth [61].

1.5.3 Identification of N-Cadherin Mimetic Peptide

Cadherin mediated cell-cell signaling has proven to be of great importance to guiding cell behavior, specifically in the context of development and regulation of cancer [22, 58]. Understanding the role of cell-cell signaling in affecting cell behaviors is of great interest to researchers. Many studies have examined cell-cell signaling in vitro by culturing cells in close proximity to one another, facilitating cadherin-mediated signaling [23, 62]. While this approach is beneficial in providing an accurate representation of cell-cell interactions in vivo, it fails to decouple cadherin-mediated cell-cell signaling from other processes involved in cell-cell interactions. To isolate the effects of cadherin mediated signaling on cell behavior, the cadherin protein, or a function amino acid sequence within the protein needs to be presented to cells. Fortunately, the amino acid sequence “HAVDI” has been identified in the region of N-cadherin that is responsible for mediating MSC cell-cell signaling [22].

1.6 Central Hypothesis

Taken together, the hypothesis of this work is that engineered cell-cell signals reduce matrix mechanosensing and this has implications in downstream cell-material

interactions. To test this hypothesis, I will pursue two specific aims. In **Aim 1**, I will develop hydrogels with HAVDI, a peptide that mimics cell-cell signals, that can stiffen on-demand using light. These hydrogels will be used for **Aim 2**, which will determine the influence of cell-cell signaling on matrix mechanosensing and on the ability of MSCs to mechanically respond to an increase in hydrogel stiffness. The ability of each hydrogel system to couple monothiol ligands to the polymer backbone and form chemical crosslinks with dithiol molecules allows for different biochemical and mechanical parameters to be explored. A hydrogel platform that can be stiffened on demand allows MSC matrix mechanosensing and mechanoadaptation to be studied within the same biomaterial system. Utilizing dynamic hydrogel systems with cell-ECM and cell-cell mimetic peptides to understand MSC behavior will provide new insights to enhance cellular expansion and provide an in vitro system that can be highly tuned to mimic specific tissue architecture.

Chapter 2 effectively demonstrated the creation of a dynamic hydrogel stiffening system biofunctionalized with peptides using two unique polymer chemistries. For the first system, hyaluronic acid (HA) was modified with methacrylate groups to form HAME macromers. Soft HAME hydrogels were formed via a Michael-addition reaction at high pH between di-thiolated crosslinkers and methacrylates in HAME macromers. These soft hydrogels were then stiffened on-demand using a photoinitiator and light, resulting in the formation of kinetic chains emanating from the methacrylate groups [63]. To biofunctionalize HAME hydrogels with thiolated peptides (e.g., adhesive RGD, cell-cell motif HAVDI), HAME macromers need to be pre-coupled with thiolated peptides via an

aqueous Michael addition reaction that binds methacrylates in HAME with thiols in thiolated peptides of interest [64].

For the second system, HA was modified with norbornene groups to form HANor macromers. In the presence of a di-thiol crosslinker, a photoinitiator, and light, soft HANor hydrogels form via click chemistry reactions between norbornenes on HANor and thiols in di-thiol crosslinkers [11]. To biofunctionalize HANor hydrogels with thiolated peptides, thiolated peptides can be mixed in the initial hydrogel solution or they can be incorporated after the hydrogel is formed, by reacting pendant, unreacted norbornenes in the HANor hydrogel network with thiolated molecules using a photoinitiator and light. Similarly, hydrogels can be stiffened at a later time by adding di-thiol crosslinkers and clicking them onto pendant norbornenes in HANor hydrogels with light [65].

Chapter 3 effectively demonstrates that substrate stiffness guides MSC behavior in the absence of other stimuli. However, high concentrations of HAVDI have a significant impact on MSC matrix mechanosensing on static substrates and in the ability for MSCs to mechanically adapt to dynamic, stiffening hydrogels. MSCs cultured on soft substrates have a small, round morphology and cytoplasmic YAP. Conversely, MSCs cultured on stiff substrates have a large, spread morphology and YAP concentrated in the nucleus. When MSCs experience elevated levels of cell-cell signaling, the characteristic response of MSCs on stiff substrates is altered. High concentrations of HAVDI cause YAP to remain in the cytosol, regardless of the substrate stiffness. Similar trends were observed when MSCs were cultured on dynamic hydrogels. When cultured on hydrogels without

HAVDI, many MSCs adapted to the stiffened hydrogel and displayed a large, spread morphology and high nuclear YAP. When HAVDI was present, fewer cells adapted to the stiff hydrogel, maintaining a small, round morphology and cytosolic YAP. The results indicate that 2 mM HAVDI is ample to overcome the mechanosensing and mechanoadaptation ability of MSCs.

Chapter 4 further examined the influence of HAVDI on MSC matrix mechanosensing and mechanoadaptation. Moving from a MeHA hydrogel system to a NorHA hydrogel system, greater control over peptide functionalization was achieved. In this chapter, HAVDI peptide concentrations of 0 mM, 0.5 mM, and 1 mM were evaluated to see if lower concentrations of HAVDI could still impact MSC behavior. On static soft hydrogels, area and morphological trends indicated no significant change in MSC behavior among HAVDI concentrations. On static stiff hydrogels, increased HAVDI resulted in significant changes to cellular area, morphology, and nuclear YAP ratio. HAVDI concentrations as low as 0.5 mM were able to significantly impact MSC behavior, suggesting that MSCs are extremely sensitive to cell-cell signaling pathways and MSCs may preferentially exclude YAP from the nucleus when faced with complete signaling pathways. Surprisingly, MSC behaved slightly different when cultured on dynamic hydrogels. Cellular area was unaffected by HAVDI concentration, and no significant difference in cellular morphology or nuclear YAP ratio was observed. Despite the lack of statistical significance, there appeared to be a correlation between HAVDI concentration and small, round MSCs with cytoplasmic YAP. These results indicate that 0.5 mM and 1 mM HAVDI influence MSC mechanoadaptation, but greater

concentrations are required to see significant changes. It is interesting to note how the same HAVDI concentrations impact MSC behavior different when cultured on static stiff versus stiffened hydrogels. Perhaps the cellular mechanisms that govern mechanosensing are slightly different from the systems that control mechanoadaptation, leading to altered effects of HAVDI concentrations.

Chapter 2

Creating Dynamic Hydrogel Systems Using Multiple Macromers

2.1 Introduction

2.1.1 Establishing a Dynamic Hydrogel System

Within the body, cells are constantly moving and being exposed to different substances. Therefore, a dynamic hydrogel system, meaning a hydrogel system that changes with respect to time, is required to more accurately study cell behavior. In this instance, the hydrogel mechanics are increasing over time, indicating a stiffening of the microenvironment. Tissue stiffening is prevalent in many disease states, such as cancer and fibrosis. In both cancer and fibrosis, lysyl oxidase crosslinking enzymes cause additional crosslinks to form between extracellular matrix proteins, collagen and elastin [66]. The secondary crosslinks contribute to stiffening of the surrounding tissue, increasing cytoskeletal tension on nearby cells, and releasing cytokines that trigger a positive feedback loop to further stiffen the tissue [66, 67].

In addition to diseased states, tissue stiffening occurs within adults as they age. Arterial stiffening is a known risk factor for cardiovascular disease and has been proven to increase with age. Collagen and elastin are important proteins in regulating the arterial elastic modulus. As an individual ages, elastin fibers can begin to break down. As elastin become less functional, the arteries begin to rely on collage for mechanical stability. The elastic modulus of collagen is significantly greater than the elastic modulus of elastin, resulting in gradual stiffening of the arterial walls [68].

With a high prevalence of tissue stiffening within the body, it is beneficial to create a hydrogel system than can accurately represent the natural progression. In the established hydrogel system, soft hydrogels are prefabricated, and cells are cultured atop the substrate. At a later time, the hydrogels are stiffened by forming additional crosslinks within the polymer network, similar to the formation of additional crosslinks seen within cancer and fibrosis tissue stiffening.

2.1.2 Methacrylated Hyaluronic Acid

Hyaluronic acid is a glycosaminoglycan that is prominently found in the cellular ECM [69]. Given its natural presence in the body, hyaluronic acid is highly biocompatible. Additionally, hyaluronic acid contains three binding groups, allowing it to be easily modified to alter its properties for specific needs [35]. For this study, methacrylated hyaluronic acid (MeHA) was created by adding methacrylates to hyaluronic acid using a reaction between methacrylate anhydride and hyaluronic acid. After the polymer was synthesized, peptides RGD and HAVDI were coupled to the polymer backbone to promote cell adhesion and imitate cell-cell signaling, respectively. Methacrylates were used because they are reactive to thiol groups and free radicals. When the polymer is introduced to a basic buffer, a Michael-type addition reaction occurs, allowing dithiol crosslinkers to form initial soft hydrogels. The mechanics of the soft hydrogels can be tuned with great specificity by altering the crosslinker concentration. The reactivity of methacrylates to free radicals allows the soft hydrogels to be stiffened at a later time point by incubating the gels in a photoinitiator solution and

exposing them to ultraviolet light. The photopolymerization creates kinetic chains across methacrylates that further stiffen the hydrogels.

2.1.3 Norbornene-Modified Hyaluronic Acid

While using MeHA hydrogels to study the effect of stiffness and cell-cell signaling on MSCs, several problems were noted. First, coupling peptides to the polymer backbone limited the control over peptide concentrations within the hydrogel. Soluble peptides were added to the soft hydrogel solution to attempt to resolve this issue, however this resulted in poor distribution of the peptides. Also, there was limited control over the elastic modulus of the stiffened hydrogel. The mechanics of the stiffened hydrogels could be altered by varying the weight percent of polymer within the hydrogel, however altering the weight percent of polymer also impacts the stiffness of the soft hydrogel, causing additional complications. Lastly, the use of two chemistries, Michael-Type addition and kinetic chain growth, is more complicated than using a single chemistry. To address these issues, the macromer was changed from MeHA to norbornene modified hyaluronic acid (NorHA). Norbornene was chosen because it has a high reactivity to thiol-radicals and a low reactivity to norbornene radicals [65]. Due to this property, radical induced click chemistry can be used to form soft hydrogels, couple monothiol peptides to the hydrogels, stiffen the hydrogels, and add peptides to preformed hydrogels. Soft NorHA hydrogel formation requires addition of a dithiol crosslinker, photoinitiator, and 10 minutes of ultraviolet radiation. Conversely, the Michael-Type addition reaction that formed MeHA hydrogels required 3 hours to complete. The drastic decrease in NorHA hydrogel formation time allows for better distribution of monothiol peptides,

possibly because they have less time to settle. In addition to better peptide distribution, NorHA provides greater control over the elastic modulus of stiffened hydrogels than MeHA. Both soft and stiff NorHA hydrogels utilize radical induced click chemistry, and the elastic modulus can be tuned by changing the DTT concentration. While both dynamic hydrogel systems can study the effects of stiffness and cell-cell signaling on MSC behavior, NorHA offers greater control over the mechanical and biochemical properties of the hydrogel.

2.2 Materials and Methods

2.2.1 MeHA Synthesis

The procedure for MeHA synthesis was based on the methodology used by Burdick et al. [70]. MeHA synthesis occurred via the esterification of the primary alcohol group at C-6 of the N-acetyl-D-glucosamine unit with methacrylic anhydride. The reaction began by dissolving hyaluronic acid and methacrylic anhydride in water, with methacrylic anhydride being added in a greater amount. The solution was kept at a pH between 8 and 10 to facilitate the reaction and neutralize methacrylic acid, which formed via a reaction between methacrylic anhydride and water and a reaction between methacrylic anhydride and hyaluronic acid [71]. The reaction occurred overnight at a temperature of 4 °C. The MeHA solution was then placed into a 6-8 kDa dialysis bag and purified by dialysis for 2 days. The purified MeHA was frozen overnight at -80 °C and freeze dried for 5 days using lyophilization (**Figure 1**). The percent modification of the HA was determined using proton nuclear magnetic resonance (H-NMR).

Figure 1

Overview of MeHA Synthesis Procedure

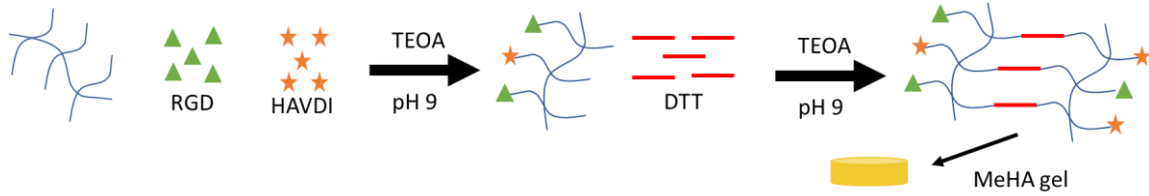


2.2.2 MeHA Hydrogel Formation

To create soft MeHA hydrogels, the polymer was dissolved in a basic solution called triethanolamine (TEOA). When the MeHA was fully dissolved, a dithiol crosslinker, dithiothreitol (DTT), was added to the hydrogel solution (**Figure 2**). The hydrogel solution was quickly added to the silicone molds, placed in a petri dish, and kept moist to prevent the hydrogels from becoming dry. Hydrogel molds were created using an 8 mm circular biopsy punch to cut sheets of silicone, for experiments with cells, or polydimethylsiloxane (PDMS), for mechanical testing. The material was then adhered to 12 mm glass coverslips to create a base for hydrogel. After 3 hours, the hydrogels are placed in a 24-well plate and soaked in phosphate buffer saline (PBS). To stiffen the hydrogels, they were first soaked a solution of PBS and photoinitiator, Irgacure-2959 (I-2959), for 30 min. Then the hydrogels were irradiated with ultraviolet light for 10 minutes at an intensity of 10 mW/cm². Following irradiation, the hydrogels were washed to remove excess free radicals and soaked in PBS.

Figure 2

Peptide Coupling to MeHA and Soft MeHA Hydrogel



2.2.3 NorHA Synthesis

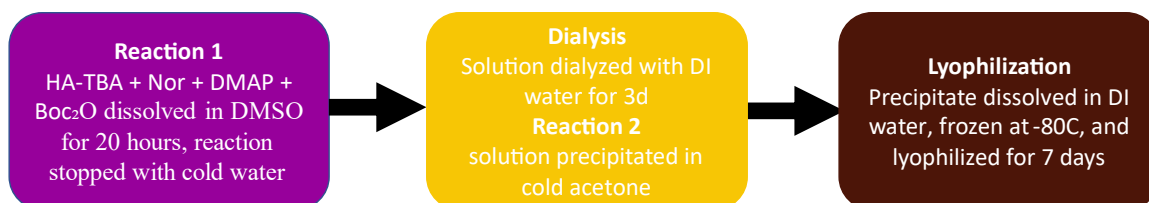
The NorHA synthesis procedure was based on the methodology laid out by Gramlich et al. [65]. Prior to creating NorHA, hyaluronic acid was transformed to its tetrabutylammonium salt (HA-TBA), permitting its solubility in dimethyl sulfoxide (DMSO). HA-TBA was created by dissolving HaNA in deionized water and adding the Dowex 50W proton exchange resin for 5 hours. After the reaction was complete, the resin was filtered out and TBA-OH was added to the solution until a pH \sim 7.03 was achieved. The solution was then frozen at -80 °C, lyophilized, and stored at -20 °C. Successful HA-TBA creation was confirmed using H-NMR analysis.

Once HA-TBA was successfully created, synthesis of the NorHA polymer began. First, a nitrogen-rich environment was created. In a flask, 2 weight percent HA-TBA was dissolved in DMSO with 5-norbornene-2-carboxylic acid, at a 3 M ratio to HA repeat units, and 4-(dimethylamino) pyridine, at a 1.5 M ratio to HA repeat units. The solution was heated to 45 °C and di-tert-butyl decarbonate (Boc_2O) was added via a syringe at a 0.4 M ratio to HA repeat units. After 20 hours, cold, deionized water was added to the solution to halt the reaction. The solution was then purified for 3 days using dialysis,

ensuring the removal of DMSO. NaCl was added to the solution at 1% w/v during dialysis and the solution was precipitated in excess cold acetone. The precipitate was dissolved in deionized water, frozen at -80 °C, lyophilized, and stored at -20°C (**Figure 3**). H-NMR analysis was performed to determine the percentage of HA repeat units modified with norbornene.

Figure 3

Overview of NorHA Synthesis Process



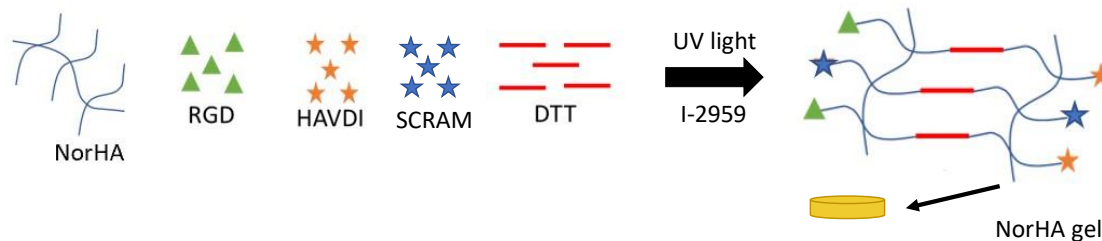
2.2.4 NorHA Hydrogel Formation

Soft NorHA hydrogels were created by first dissolving the macromer in PBS. Solubilized peptides, including RGD, HAVDI, and scrambled HAVDI, were then added to the solution and mixed to ensure even dispersion. All hydrogels had a total peptide concentration of 2 mM, with 1 mM RGD being constant among all hydrogels. The HAVDI concentration varied among 0 mM, 0.5 mM, and 1 mM. The hydrogels without 1 mM HAVDI contained scrambled-HAVDI in various concentrations to provide a total peptide concentration of 2 mM. Next, DTT and I-2959 are added to the solution, briefly mixed, and pipetted into silicone molds. Hydrogel molds were created using an 8 mm

circular biopsy punch to cut sheets of silicone, for experiments with cells, or PDMS, for mechanical testing. The material was then adhered to 12 mm glass coverslips to create a base for hydrogel. Once inside the molds, the hydrogel solution was irradiated with ultraviolet light for 10 minutes at an intensity of 10 mW/cm² (**Figure 4**). Following irradiation, the hydrogels were washed to remove excess free radicals and soaked in PBS. The hydrogels were stiffened by soaking them in a solution containing PBS, DTT, and I-2959 for 30 minutes and then exposing the hydrogels to ultraviolet light for 10 minutes at an intensity of 10 mW/cm². The stiffened hydrogels were then washed to remove remaining free radicals and soaked in PBS.

Figure 4

Overview of the Soft NorHA Hydrogel Formation Process



2.2.5 Scrambled HAVDI Synthesis

The sequence for scrambled HAVDI was based on the study by Cosgrove et al. [22]. The peptide went through F-moc solid phase peptide synthesis using DMF as a solvent. A special aspartic acid, called ASP_OMPe was used to prevent aspartame formation. Additionally, 10% piperazine was dissolved in solution that contained 90% N-methyl

pyrrodine and 10% ethanol. An additional 0.1 M of Oxyma was added to the deprotection solution. The activator and activator base used were 1 M DIC and 1 M Oxyma pure, respectively. Synthesis occurred in the Liberty Blue peptide synthesizer. The coupling required 4 minutes at 90 °C for all amino acids, except for aspartic acid, which occurred for 4 minutes at room temperature. The peptide was cleaved for 3 hours in a cocktail solution consisting of 92.5% TFA, 2.5% DoDt, 2.5% Tiis, and 2.5% H₂O and then precipitated six times using cold diethyl ether. The peptide dried overnight, was purified using a 0.2 µm filter, frozen at -80 °C, lyophilized, and stored at -20 °C. The molecular weight of the peptide was determined using MALDI analysis.

2.2.6 Mechanical Testing of Hydrogels

Compressive testing was used to calculate the elastic moduli of hydrogels via a Shimadzu EZ Test machine. The hydrogels had an average diameter of 8 mm and an average height of 1.7 mm. The strain rate of the mechanical tester was fixed at 10% strain/ minute for all experiments and test ended when 30% strain was reached. The elastic modulus was calculated from the slope of a stress-strain curve between 10% and 20% strain rate.

2.3 Results and Discussion

2.3.1 H-NMR Analysis of MeHA

Successful coupling of methacrylate groups to hyaluronic acid was confirmed by H-NMR analysis (**Figure 5A**). The chemical groups corresponding to each peak were compared to the MeHA H-NMR from Guvendiren & Burdick [35]. There are several peaks that indicate hyaluronic acid, including peaks between 3.0 and 4.0 ppm, peaks ~4.5

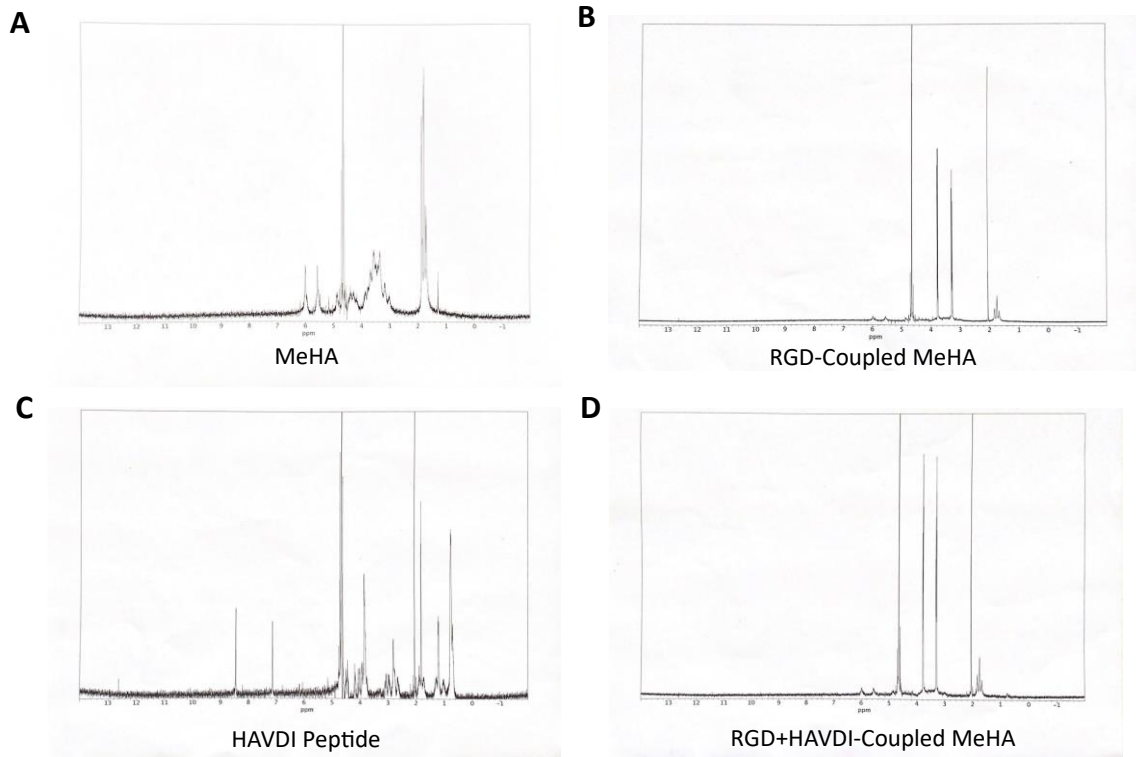
ppm, and peaks ~5 ppm. The smaller peaks ~2 ppm indicate protons associated with methyl groups on hyaluronic acid and methacrylates. The peaks between 5.5 and 6.5 ppm indicate protons associated with the alkene groups on methacrylates [35]. The presence of these peaks verify that MeHA was successfully created.

After a large batch of MeHA was synthesized, it was divided into smaller groups that were coupled to peptides. One group contained 2 mM RGD, and the other group contained 2 mM RGD and 2 mM HAVDI. Successful coupling of RGD to both groups was confirmed by comparing the integration values of the peaks located between 5.5 and 6.5 ppm, which are indicative of methacrylate groups (**Figures 5B & D**). The ability of H-NMR to detect methacrylate groups when bound to RGD decreases, reducing the integration values at the methacrylate peaks. Both RGD- and RGD+HAVDI-coupled MeHA display a decreased integration value compared to uncoupled MeHA at peaks between 5.5 and 6.5 ppm.

Lastly, successful coupling of HAVDI to the RGD+HAVDI-coupled MeHA was confirmed by identifying a unique peak on this MeHA group and comparing it to the peaks of solubilized HAVDI. A peak ~1 ppm was identified on the RGD+HAVDI-coupled MeHA that was not found on any other MeHA group (**Figure 5D**). The peak was also present on the H-NMR analysis of solubilized HAVDI, confirming that a peak ~1 ppm is indicative of HAVDI, and that HAVDI was successfully coupled to the MeHA (**Figure 5C**).

Figure 5

H-NMR Analysis of MeHA



Note. H-NMR results of (A) MeHA, (B) MeHA coupled with RGD, (C) HAVDI peptide, and (D) MeHA coupled with RGD and HAVDI.

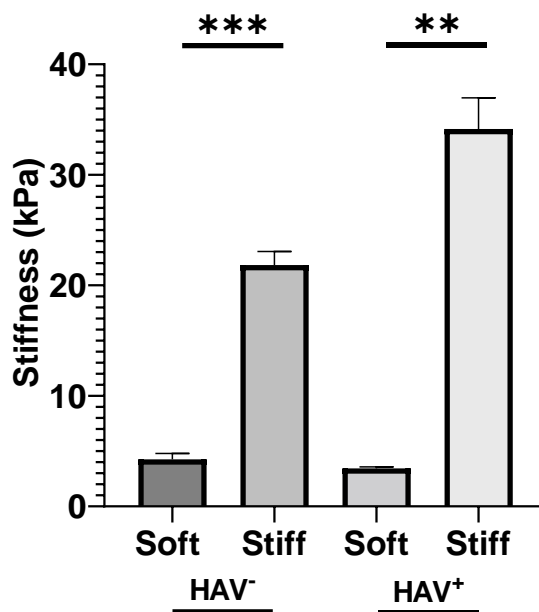
2.3.2 Mechanical Characterization of MeHA

Two MeHA batches were analyzed for mechanical characterization, RGD-coupled MeHA and RGD+HAVDI-coupled MeHA. For both groups, distinct soft and stiff hydrogels were required to establish a dynamic hydrogel system. The target stiffness for soft hydrogel was ~2-3 kPa and the desired stiffness for stiff hydrogels was ~20-30 kPa. These values highlighted a 10-fold increase in stiffness between soft and stiff hydrogels, which have proven to have significantly different effects on MSCs in previous

mechanical studies [11]. Soft hydrogel stiffness was changed primarily by altering the DTT concentration of the hydrogel because it provided the great control over stiffness. However, stiffness could also be affected by changing the weight percent of the macromer. Due to the kinetic chain growth reaction, the elastic moduli of stiff hydrogels were only controlled by altering macromer weight percent, which also influenced soft hydrogel elastic moduli. After evaluating several DTT concentrations and macromer weight percentages, the optimal parameters for soft and stiff hydrogels were found to be 4 wt % MeHA and 5 mM DTT. These conditions resulted in soft hydrogels with an average elastic modulus of 4.25 kPa for RGD-coupled MeHA and 3.44 kPa for RGD+HAVDI-coupled MeHA. The stiff hydrogels had an average elastic modulus of 21.83 kPa for RGD-coupled MeHA and 31.14 kPa for RGD+HAVDI coupled MeHA (**Figure 6**). The stiff RGD-coupled MeHA hydrogels and the stiff RGD+HAVDI-coupled MeHA hydrogels were significantly stiffer than their respective soft hydrogels.

Figure 6

Mechanical Characterization of MeHA Hydrogels



Note. Elastic modulus of soft and stiff hydrogels with and without 2mM HAVDI. All hydrogels contain 2mM RGD. Bar graphs represent the mean; **p < 0.01, ***p < 0.001.

2.3.3 H-NMR Analysis of NorHA

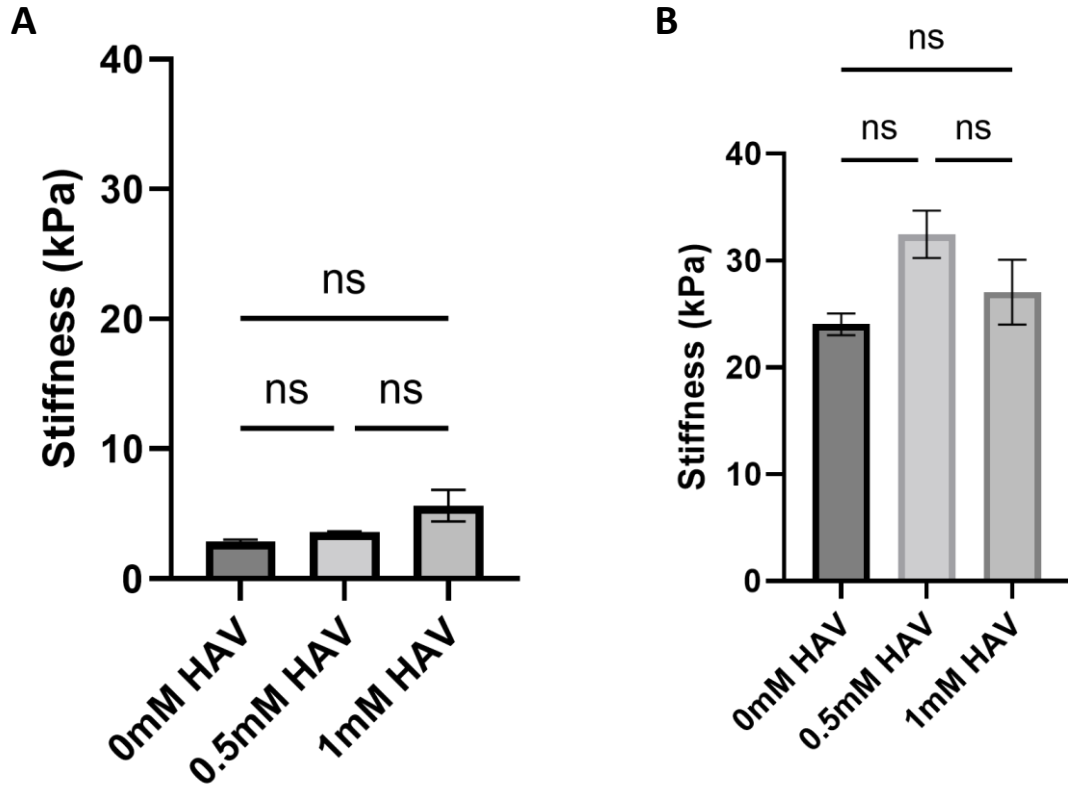
Verification of successful NorHA synthesis required two steps, H-NMR analysis of HA-TBA and NorHA. The H-NMR spectra of HA-TBA was compared to the results from a study by Gramlich et al. [65]. The characteristic peaks of HA-TBA found ~3.2 ppm, ~1.68 ppm, ~1.40 ppm, and ~0.97 ppm was also found on the HA-TBA used in this study, indicating successful creation of the salt (**Figure 7A**).

NorHA H-NMR displayed peaks between 3.0 and 4.0 ppm, ~4.5 ppm, and ~5 ppm, which are indicative of hyaluronic acid. Additionally, peaks were found ~2 ppm, and between 5.6 and 6.2 ppm, which indicate hyaluronic acid methyl groups and norbornene,

hydrogels was ~20-30 kPa. NorHA hydrogels were both formed and stiffened using a radical-induced thiol-norbornene reaction. This reaction allowed the elastic moduli of soft and stiff hydrogels to be tuned by altering DTT concentration. Soft and stiff hydrogels with varying DTT concentration were evaluated until an optimal elastic modulus was found. All hydrogels were formed using 3 wt% NorHA. Soft hydrogels had a DTT concentration of 0.5 mM and stiff hydrogels had a total DTT concentration of 3mM, with 0.5mM DTT used to form soft hydrogels and an additional 2.5 mM DTT used to stiffen the hydrogels. Soft hydrogels had an average stiffness between 2.8 kPa and 5.6 kPa, with no significant difference observed among HAVDI concentrations (**Figure 8A**). Stiff hydrogels had an average stiffness between 24.0 kPa and 32.5 kPa, with no significant difference observed among HAVDI concentrations (**Figure 8B**).

Figure 8

Mechanical Characterization of NorHA Hydrogels



Note. Elastic modulus of (A) soft and (B) stiff NorHA hydrogels with varying concentrations of HAVDI. All hydrogels have 1mM RGD and a total peptide concentration of 2mM. Scrambled HAVDI is added to hydrogels with less than 1mM HAVDI to reach a total concentration of 2mM. Bar graphs represent the mean; ns, not significant.

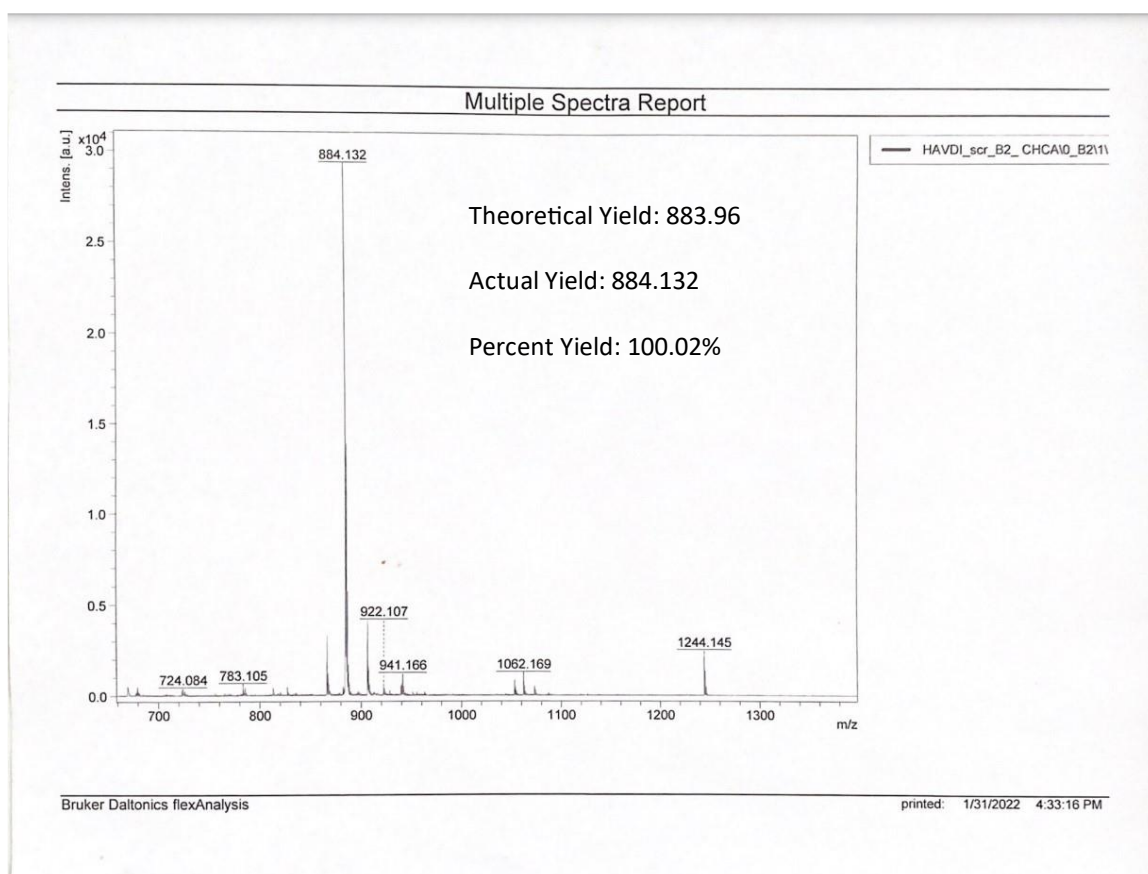
2.3.5 MALDI Analysis of Scrambled HAVDI

MALDI was used to determine the actual molecular weight of the scrambled HAVDI peptide created by the peptide synthesizer and compare that value to the theoretical molecular weight of the scrambled HAVDI. The theoretical molecular weight of the scrambled HAVDI peptide was 883.96 Da and the measured molecular weight of the

peptide was 884.132 Da, as indicated by the value of the peak. The percent yield calculated from these values was 100.02% (**Figure 9**).

Figure 9

MALDI Analysis of the Scrambled HAVDI Peptide



Chapter 3

MeHA Hydrogels to Evaluate the Effect of HAVDI on MSCs

3.1 Overview

The effect of 2D hydrogel stiffness on MSC behavior has been well characterized. Soft hydrogels promote a small, round morphology and adipogenic differentiation, whereas stiff hydrogels guide MSCs towards a large, spread phenotype that favors osteogenic differentiation. In addition to substrate stiffness, cell-cell signaling is known to heavily influence MSC behavior. Cosgrove et al. showed that hydrogels containing 1 mM RGD and 1 mM HAVDI were able to significantly reduce the nuclear YAP of MSCs on hydrogels with elastic moduli between 10-15 kPa [22]. This information was combined to create a hydrogel system that can be stiffened on demand to evaluate the effect of HAVDI on MSCs in both static and dynamic environments.

3.2 Materials and Methods

3.2.1 MSC Culture

Bone marrow derived MSCs were purchased from Lonza and reached a passage number between P2 and P5 prior to seeding. MSCs were stored in liquid nitrogen at a cell density of 500,000 cells/vial. Cells were thawed and expanded on TCP dishes prior to experimentation. MSCs were cultured with alpha minimum essential media containing streptomycin, penicillin, and 10% fetal bovine serum (FBS). Cells were expanded until 80%-90% confluency before passaging or seeding. When the cells reached the desired confluency, they were washed with PBS and then incubated with trypsin for 5 minutes to

facilitate cellular detachment from the TCP. Media was then added to the cells to offset the effects of the trypsin. The MSCs, media, and trypsin were combined in a conical tube and centrifuged at 500g for 5 minutes. The supernatant was then removed, and the remaining cell pellet was resuspended in media. The cells were counted using a hemacytometer and then seeded on hydrogels, passaged to a new petri dish, or refrozen in liquid nitrogen.

3.2.2 MSC Staining

After the MSCs were cultured on hydrogels for a set length of time, they were fixed and stained. The MSCs were fixed by incubating them 10% formalin for 10 minutes. The hydrogels were then washed and a permeabilization solution, consisting of a 1:10 dilution of Triton-X in PBS, was added to each hydrogel for 3 minutes. The MSCs were washed again and then a blocking buffer was added to each hydrogel for 30 minutes. The blocking buffer was created by dissolving 3 wt% bovine serum albumin (BSA) in PBS. While the MSCs were in the blocking buffer, a primary YAP solution was prepared using a 1:200 dilution of mouse IgG YAP antibodies in blocking buffer. After blocking was completed, the primary YAP solution was added to the MSCs, and cells were stored in darkness for 1 hour. The hydrogels were then washed four times to remove excess antibodies. During the washing steps, a secondary YAP solution was prepared using a 1:200 dilution of anti-mouse IgG antibodies in blocking buffer. The MSCs were incubated with the secondary YAP solution after the washing was complete and stored in darkness for 2 hours. The hydrogels were then washed five times and a phalloidin solution was created using a 1:200 dilution of 568 wavelength phalloidin in blocking

buffer. The hydrogels were soaked in the phalloidin solution for 15 minutes in and then washed twice. A Hoechst solution was prepared using a 1:2500 dilution of Hoechst in PBS and the solution was added to the MSCs for 5 minutes. The hydrogels were then washed twice, and the well-plate was wrapped in foil and stored in 4 degrees Celsius until imaging.

3.2.3 Imaging and Analysis

Hydrogel surface imaging was conducted on a Confocal Microscope using the 20x objective lens. Cellular analysis was completed using the Fiji is just ImageJ (FIJI) software. The nuclear YAP concentrations of MSCs were calculated in several steps. First, masks of the cytoplasm and nucleus of the cell were created using the phalloidin and Hoechst channels. These masks were placed atop the YAP channel to obtain a nuclear and cellular YAP intensity, and each intensity was normalized to its respective area. The normalized nuclear YAP was then divided by the normalized cellular YAP to obtain a nuclear-to-cellular YAP ratio. In addition to nuclear YAP ratios, cellular and nuclear size and morphology were characterized by separating the phalloidin and Hoechst channels, converting the image to black-and-white, and using FIJI's inherent measuring tools.

3.2.4 Statistical Analysis

Statistical analysis for data comparing two variables, an unpaired t test was used, assuming equal standard deviations. When examining three or more variables, an ANOVA test followed by a post-hoc Tukey test was used,

3.3 Results and Discussion

3.3.1 Static MSC Area Analysis on MeHA

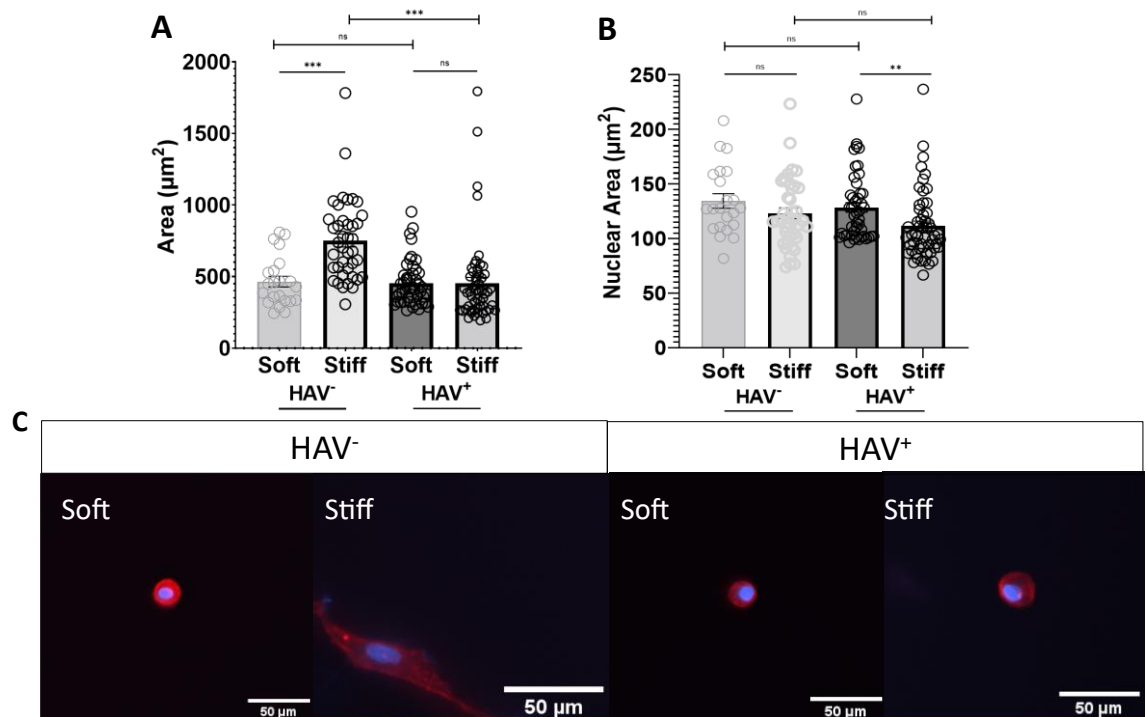
When the hydrogels contained 0 mM HAVDI, MSC cellular area was significantly greater on stiff hydrogels than on soft hydrogels. MSCs cultured on soft hydrogels had an average cellular area $\sim 460 \mu\text{m}^2$ and MSCs cultured on stiff hydrogels had an average cellular area $\sim 750 \mu\text{m}^2$. However, this trend did not exist when hydrogels were created with 2 mM HAVDI. When hydrogels contained 2 mM HAVDI, MSCs cultured on stiff hydrogels were not significantly larger than MSCs cultured on soft hydrogels. MSCs cultured on soft hydrogels with had an average cellular area $\sim 454 \mu\text{m}^2$ and MSCs cultured on stiff hydrogels had an average cellular area of $\sim 453 \mu\text{m}^2$ (**Figure 10A & C**). The presence of HAVDI in soft hydrogels had a nonsignificant impact on cellular area. However, the presence of HAVDI in stiff hydrogels had a significant impact on cellular area. The presence of HAVDI significantly reduces average MSC cellular area on stiff hydrogels. These results indicate that the cell-cell signaling from 2 mM HAVDI reduces the matrix mechanosensing ability of the cells, preventing them from increasing in size on stiff hydrogels.

Unlike cellular area, nuclear area did not appear to be significantly impacted by hydrogel stiffness. MSC nuclear area on soft and stiff hydrogels was not significantly different, when neither hydrogel contained HAVDI. The addition of HAVDI did not appear to impact nuclear area. No significant difference was observed between soft hydrogels with and without HAVDI or stiff hydrogels with and without HAVDI. MSC nuclear area was significantly smaller on stiff hydrogels than soft hydrogels, when both

substrates contained 2 mM HAVDI (**Figure 10B & C**). This result may be attributed to cell-to-cell variability in nuclear size, and future studies could be designed towards understanding this interesting phenomenon.

Figure 10

Cellular and Nuclear Area of MSCs on Static MeHA Hydrogels



Note. (A) Cellular and (B) nuclear area quantification of MSCs cultured on soft and stiff MeHA hydrogels with 0mM or 2mM HAVDI. (C) Representative images of MSCs (red, actin; blue, nuclei) cultured on soft and stiff hydrogels with 0mM or 2mM HAVDI. Bar graphs represent the mean and points individual cells; ns, not significant, ** $p < 0.01$, *** $p < 0.001$.

3.3.2 Static MSC Morphology Analysis on MeHA

In addition to cellular area, MSC morphology was assessed to evaluate the effect of HAVDI on MSC behavior. Two metrics were used to quantify MSC morphology, circularity, and aspect ratio. Circularity was quantified with a number between 0 and 1. A value of 1 indicates a perfect circle and values approaching 0 indicate an elongated shape. Aspect ratio is measured by dividing the cell's major axis by its minor axis. A larger aspect ratio corresponds to a more elongated object, whereas a smaller aspect ratio indicates a more rounded object. Using circularity and aspect ratio, changes in MSC morphology were able to be characterized.

There was a significant difference in MSC cellular circularity between soft and stiff hydrogels with 0 mM HAVDI. MSCs cultured on soft hydrogels had an average cellular circularity of 0.79 and MSCs cultured on stiff hydrogels had an average cellular circularity of 0.45. When hydrogels contained 2 mM HAVDI, there was a nonsignificant difference in average cellular circularity between MSCs on soft and stiff hydrogels. Soft hydrogels had an average cellular circularity of 0.78 and stiff hydrogels had an average cellular circularity of 0.77 (**Figure 11A**). The presence of HAVDI in soft hydrogels had a nonsignificant impact on cellular circularity. However, the presence of HAVDI in stiff hydrogels had a significant impact on cellular circularity.

While the presence of HAVDI increased MSC cellular circularity on stiff hydrogels, it simultaneously decreased the aspect ratio of MSCs. When hydrogels contained 0 mM HAVDI, there was a significant increase in cellular aspect ratio between MSCs cultured on soft and stiff hydrogels. MSCs cultured on soft hydrogels had an average cellular

aspect ratio of 1.47, and MSCs cultured on stiff hydrogels had an average cellular aspect ratio of 3.45. When hydrogels contained 2 mM HAVDI, there was no significant difference observed between MSC cellular aspect ratio on soft and stiff hydrogels. Soft hydrogels had an average cellular aspect ratio of 1.46 and stiff hydrogels had an average cellular aspect ratio of 1.57 (**Figure 11B**). The presence of HAVDI in soft hydrogels had a nonsignificant impact on cellular aspect ratio. However, the presence of HAVDI in stiff hydrogels had a significant impact on cellular aspect ratio.

The same trends were observed in cellular circularity were also observed in nuclear circularity. MSC nuclei on stiff hydrogels were significantly less circular than MSC nuclei on soft hydrogels, when 0mM HAVDI were present. MSCs cultured on soft hydrogels had an average nuclear circularity ~0.85 and MSC cultured on stiff hydrogels had an average nuclear circularity ~0.82. Additionally, there was a significant difference in nuclear circularity between stiff hydrogels with and without 2 mM HAVDI. MSCs cultured on stiff hydrogels with 2 mM HAVDI had an average nuclear circularity ~0.87 (**Figure 11C**). The increase in nuclear circularity indicates that HAVDI helped drive MSC nuclei towards a round morphology. To help verify this claim, nuclear morphology was analyzed further using aspect ratio.

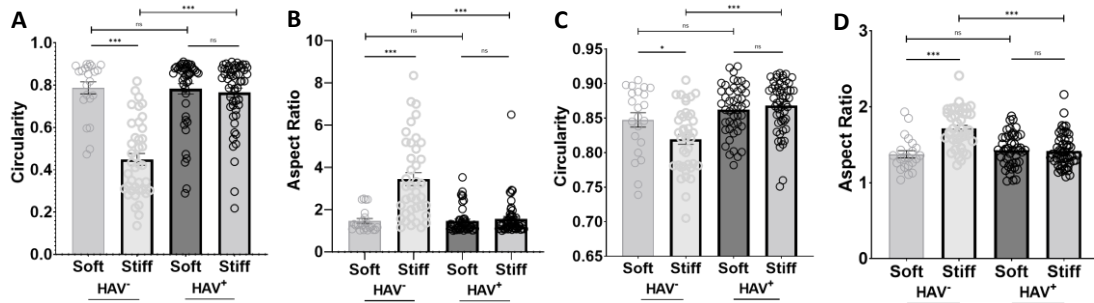
Nuclear aspect ratio was also impacted by hydrogel stiffness and the presence of HAVDI. Without HAVDI, MSC nuclei had a significantly greater aspect ratio when cultured on stiff hydrogels than when cultured on soft hydrogels. MSCs cultured on soft hydrogels has an average nuclear aspect ratio ~1.37 and MSCs cultured on stiff hydrogels had an average nuclear aspect ratio ~1.72. When MSCs were cultured on stiff hydrogels

containing 2 mM HAVDI, the nuclear aspect ratio significantly decreased relative to MSCs cultured on stiff hydrogels without HAVDI. MSCs cultured on stiff hydrogels with 2mM HAVDI had an average nuclear aspect ratio ~ 1.42 (**Figure 11D**). This evidence suggests that the HAVDI peptide played a role in decreasing nuclear spreading.

Combining the cellular and nuclear morphology, it is evident that 2 mM HAVDI significantly affects the physical shape of MSCs and their nuclei on stiff hydrogels. Thus far, the addition of 2 mM HAVDI to stiff hydrogels has significantly decreased cellular area, increased cellular and nuclear circularity, and decreased cellular and nuclear aspect ratio. The presence of HAVDI lead the cells towards a small and round morphology, which corresponds with MSCs cultured on a soft hydrogel. Therefore, HAVDI reduced MSCs' ability to interpret signals from their environment. To further understand how HAVDI drives these physical changes, a protein regulator of matrix mechanosensing, YAP, must be analyzed.

Figure 11

Cellular and Nuclear Morphology of MSCs on Static MeHA Hydrogels



Note. Cellular (A) circularity and (B) aspect ratio of MSCs cultured on soft and stiff MeHA hydrogels with 0 mM or 2 mM HAVDI. Nuclear (C) circularity and (D) aspect ratio of MSCs cultured on soft and stiff MeHA hydrogels with 0 mM or 2 mM HAVDI. Bar graphs represent the mean and points individual cells; ns, not significant, * $p < 0.05$, *** $p < 0.001$.

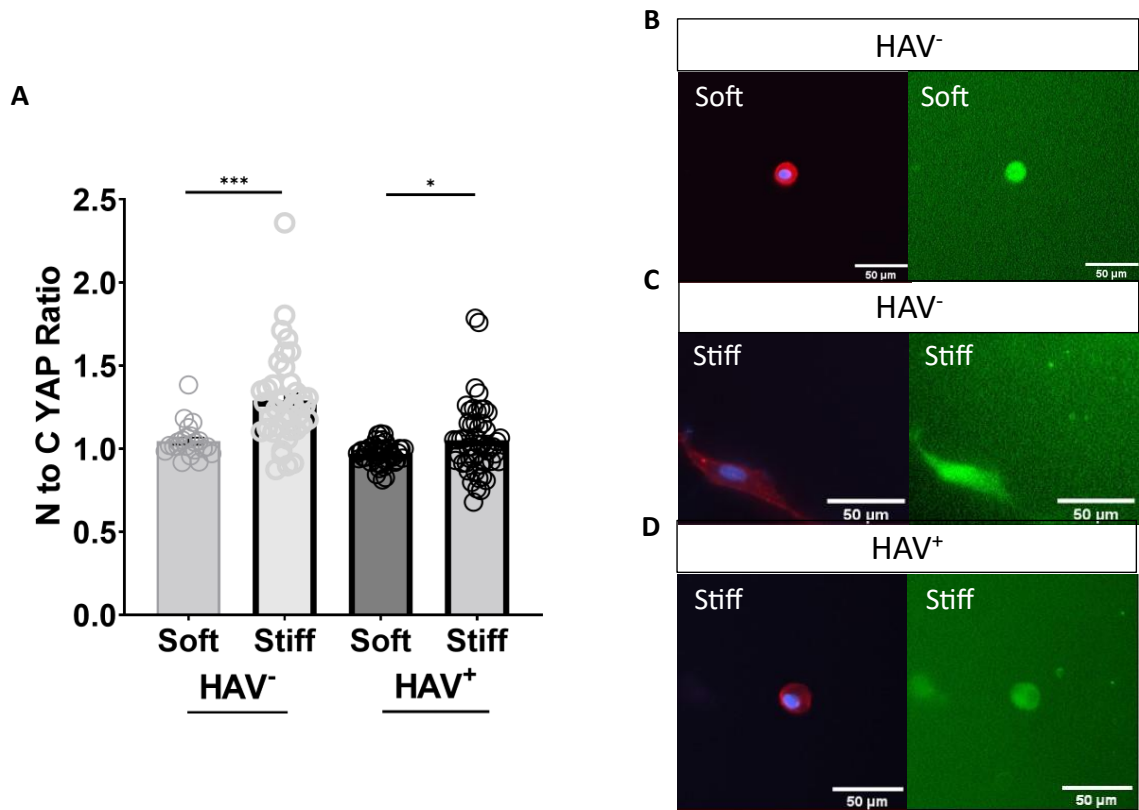
3.3.3 Static MSC Nuclear YAP Analysis on MeHA

After quantifying the physical traits of MSCs, it is important to understand the cellular mechanism behind the observed behavior. YAP is a mechanosensitive protein that is present throughout the cytosol when a cell is not under mechanical stress. When the cell exerts a force on its surroundings, YAP relocates to the nucleus, allowing the cell to transduce mechanical stimuli from the environment into chemical signals within the cell [28]. When hydrogels contained 0 mM HAVDI, MSCs on soft hydrogels have an average nuclear YAP ratio of ~ 1.05 , and MSCs on stiff hydrogels have an average nuclear YAP ratio ~ 1.29 . There was a significant difference in nuclear YAP between soft and stiff hydrogels, confirming that stiffness promotes an increase in nuclear YAP (Figures 12B & C). When hydrogels contained 2 mM HAVDI, there was also a significant difference in nuclear YAP between soft and stiff hydrogels. This suggests that

hydrogel stiffness influences nuclear YAP, even when HAVDI is present. When HAVDI is present, MSCs on soft hydrogels have an average nuclear YAP ~0.97 and MSCs on stiff hydrogels have an average nuclear YAP ~1.05 (**Figure 12A**). While HAVDI does not completely overcome the effect of stiffness on nuclear YAP, the peptide does cause a significant effect. The nuclear YAP of MSCs cultured on stiff hydrogels without HAVDI was significantly greater than the nuclear YAP of MSCs cultured on stiff hydrogels with HAVDI (**Figure 12D**). An interesting future study could examine nuclear YAP localization when MSCs are cultured on a stiff substrate with a greater concentration of HAVDI (e.g., 5 mM) to determine if nuclear YAP could be decreased to the level of MSCs cultured on soft hydrogels. Taken together, HAVDI and hydrogel stiffness appear to play significant roles in guiding nuclear YAP localization.

Figure 12

Nuclear YAP of MSCs Cultured on Static MeHA Hydrogels



Note. (A) Nuclear to cytoplasmic YAP ratios of MSCs cultured on soft and stiff MeHA hydrogels with 0 mM or 2 mM HAVDI. Representative images of MSCs (red, actin; blue, nuclei; green, YAP) cultured on (B) soft hydrogels with 0mM HAVDI, (C) stiff hydrogels with 0 mM HAVDI, and (D) stiff hydrogels with 2 mM HAVDI. Bar graphs represent the mean and points individual cells; * $p < 0.05$, *** $p < 0.001$.

3.3.4 Dynamic MSC Area Analysis on MeHA

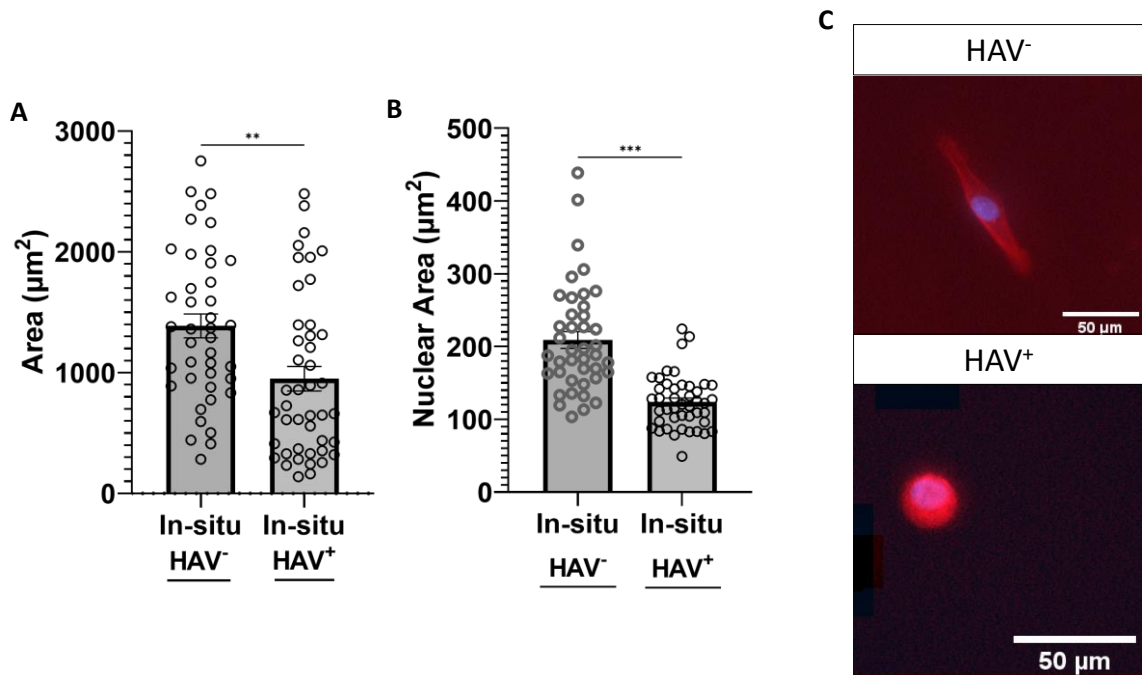
After MSCs were analyzed to evaluate the effect of stiffness and HAVDI on MSC behavior on static hydrogels, hydrogels were stiffened in real-time to determine the effect of HAVDI on mechanoadaptation from the in-situ transition from a soft to a stiff environment. Dynamic hydrogels were cultured for a total of 2 days, 1 day on the soft

hydrogel and 1 day on the stiffened hydrogel. When hydrogels were stiffened without HAVDI, MSC area was widely distributed. Some cells adapted to the stiff hydrogel while other cells remained small due to the mechanical memory of the soft hydrogels. When the hydrogels contained HAVDI, MSC area was still widely distributed, but average cell area was significantly smaller than MSCs cultured on hydrogels without HAVDI. The average cellular area of MSCs cultured on dynamic hydrogels without HAVDI was $\sim 1,387\mu\text{m}^2$ and the average cellular area of MSCs culture on dynamic hydrogels with HAVDI was $\sim 950\mu\text{m}^2$ (**Figures 13A & C**). The presence of HAVDI within dynamic hydrogels appeared to limit MSCs ability to mechanical adapt to a stiff substrate.

The nuclear area of MSCs cultured on stiffened hydrogels was also impacted by HAVDI. When hydrogels were stiffened without the presence of HAVDI, MSCs displayed a disperse range of nuclear areas and the average nuclear area was $\sim 209\mu\text{m}^2$. When hydrogels containing HAVDI were stiffened, the nuclear area was less dispersed than when HAVDI was not present, and the average nuclear area was $\sim 124\mu\text{m}^2$ (**Figures 13B & C**). A significant difference in nuclear area was observed between MSCs cultured on stiffened hydrogels with and without HAVDI. These results suggest that the presence of HAVDI impact MSC nuclei during mechanoadaptation.

Figure 13

Cellular and Nuclear Area of MSCs on Dynamic MeHA Hydrogels



Note. (A) Cellular and (B) nuclear area quantification of MSCs cultured on dynamic (in situ) MeHA hydrogels with 0mM or 2mM HAVDI. (C) Representative images of MSCs (red, actin; blue, nuclei) cultured on dynamic hydrogels with 0mM or 2mM HAVDI. Bar graphs represent the mean and points individual cells; ** $p < 0.01$, *** $p < 0.001$.

3.3.5 Dynamic MSC Morphology Analysis on MeHA

In addition to area analysis, cellular and nuclear morphology analysis was completed to evaluate the effect of HAVDI on mechanoadaptation. The average circularity of MSCs cultured on stiffened hydrogels without HAVDI was ~ 0.35 . Most cells of the displayed a low circularity, suggesting that the majority of MSCs adapted to the stiff substrate. Cellular circularity was significantly greater for MSCs cultured on dynamic hydrogels with 2mM HAVDI than MSC cultured on dynamic hydrogels without HAVDI. The

average cellular circularity for MSCs cultured on stiffened gels with HAVDI was ~ 0.52 (**Figure 14A**). When HAVDI was present, the MSCs displayed a wide range of circularity values, which suggests that fewer cells were adapting to the stiff hydrogel because of the HAVDI interactions.

MSC aspect ratio was evaluated to further identify morphology trends affected by HAVDI. There was a significant difference between MSCs cultured on dynamic hydrogels with HAVDI and without HAVDI. The average cellular aspect ratio of MSCs cultured on dynamic hydrogels without HAVDI was ~ 3.32 and the average cellular aspect ratio of MSCs cultured on dynamic hydrogels with HAVDI was ~ 2.25 (**Figure 14B**). Without HAVDI, MSCs on dynamic hydrogels displayed a wide range of cellular aspect ratios, which indicated that cells were adapting to the stiffened hydrogel to varying degrees. With HAVDI, most cells on dynamic hydrogels displayed a low cellular aspect ratio, although some cells appear spread. The decrease in the number of cells that express a high aspect ratio indicates that HAVDI interferes with MSC mechanoadaptation.

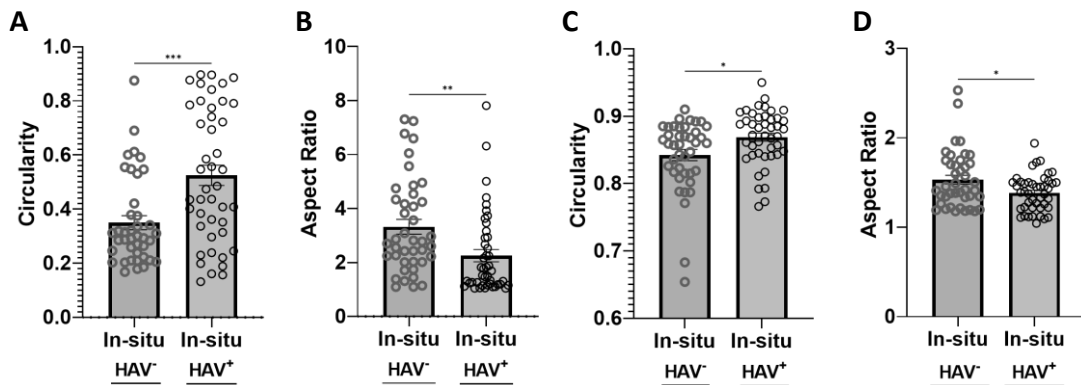
MSC nuclear circularity displayed similar trends to MSC cellular circularity on dynamic hydrogels. The nuclear circularity of MSCs cultured on stiffened hydrogels without HAVDI was significantly lower than the nuclear circularity of MSCs cultured on stiffened hydrogels with HAVDI. The average nuclear circularity of MSCs cultured on stiffened hydrogels without HAVDI was ~ 0.84 and the average nuclear circularity of MSCs cultured on stiffened hydrogels with HAVDI was ~ 0.87 (**Figure 14C**). The correlation between nuclear circularity on dynamic hydrogels and the presence of

HAVDI suggests that HAVDI reduces MSC nuclei ability to mechanically adapt to a stiffened substrate.

MSC nuclear aspect ratio was also influenced by the interactions with HAVDI. MSCs cultured on stiffened hydrogels without HAVDI displayed a significantly larger aspect ratio than MSCs cultured on stiffened hydrogels with HAVDI. The average nuclear aspect ratio of MSCs cultured on dynamic hydrogels without HAVDI was ~1.53, and the average nuclear aspect ratio of MSCs cultured on dynamic hydrogels with HAVDI was ~1.38 (**Figure 14D**). The decrease in nuclear aspect ratio when HAVDI is present further supports that claim that HAVDI reduced the mechanoadaptation of MSCs on dynamic hydrogels.

Figure 14

Cellular and Nuclear Morphology of MSCs on Dynamic MeHA Hydrogels



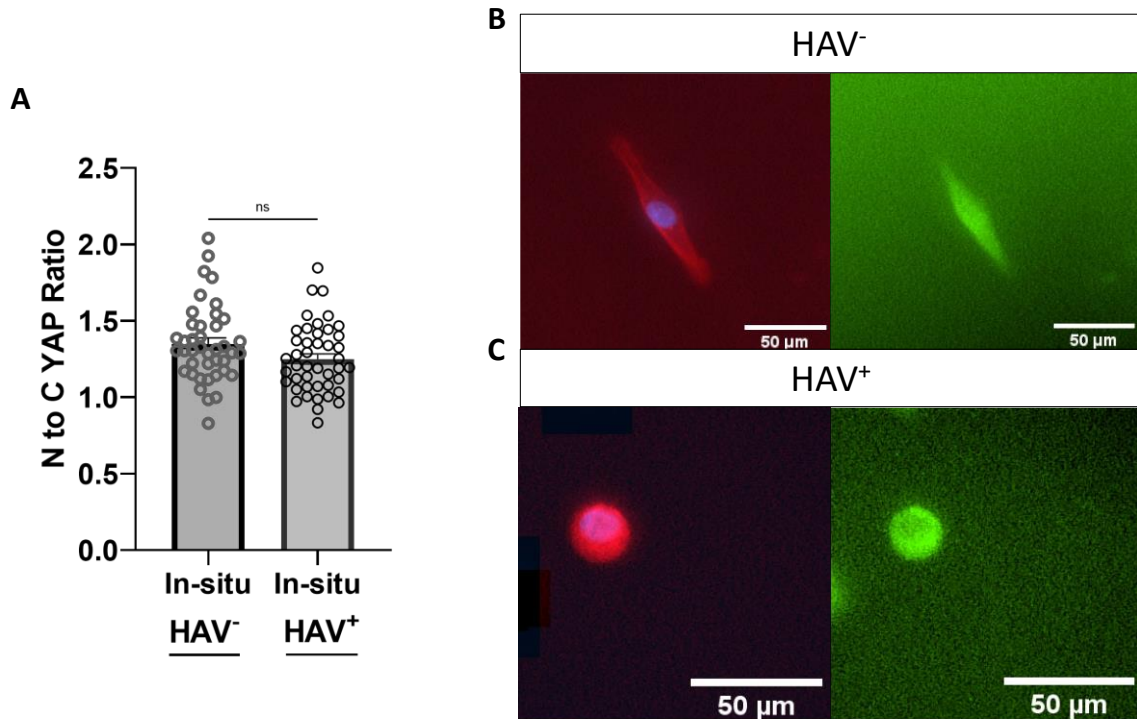
Note. Cellular (A) circularity and (B) aspect ratio of MSCs cultured dynamic (in situ) MeHA hydrogels with 0 mM or 2 mM HAVDI. Nuclear (C) circularity and (D) aspect ratio of MSCs cultured on dynamic (in situ) MeHA hydrogels with 0mM or 2 mM HAVDI. Bar graphs represent the mean and points individual cells; * $p < 0.05$, ** $p < 0.01$, *** $p < 0.001$.

3.3.6 Dynamic MSC Nuclear YAP Analysis on MeHA

To better understand how stiffness and cell-cell signaling impact MSC mechanoadaptation, YAP was assessed because it is a regulator of cellular mechanosensing. When MSCs were cultured on stiffened hydrogels contained 0mM HAVDI, nuclear YAP ratios were widely dispersed, which demonstrated varying degrees of adaptation. The average nuclear YAP ratio was ~1.35. When dynamic hydrogels contained 2mM HAVDI, the nuclear YAP values were less dispersed, and the average nuclear YAP value fell to ~1.25 (**Figure 15A-C**). While there was not a significant difference observed between dynamic hydrogels with and without HAVDI, nuclear YAP values appear to be decreasing when HAVDI is present. Perhaps increasing the culture time would allow more cells to develop more a pronounced adaptation to the stiffened substrate and create a significant difference in nuclear YAP between dynamic hydrogels with and without HAVDI.

Figure 15

Nuclear YAP of MSCs Cultured on Dynamic MeHA Hydrogels



Note. (A) Nuclear to cytoplasmic YAP ratios of MSCs cultured on dynamic (in situ) MeHA hydrogels with 0mM or 2mM HAVDI. Representative images of MSCs (red, actin; blue, nuclei; green, YAP) cultured on (B) dynamic hydrogels with 0mM HAVDI and (C) dynamic hydrogels with 2mM HAVDI. Bar graphs represent the mean and points individual cells; ns, not significant.

3.4 Conclusion

Based on the results from Chapter 3, and findings from previous studies, it is evident that stiffness plays a prominent role in guiding MSC behavior. When HAVDI is not present in static hydrogels, and stiffness is the primary factor influencing MSC behavior, cells display characteristic responses. When cultured on soft hydrogels, MSCs cellular and nuclear morphology is small and round, and YAP resides within the cytoplasm.

Conversely, when MSCs are cultured on stiff hydrogels, MSCs display a large, spread cellular and nuclear morphology and YAP localizes within the nucleus. When HAVDI is introduced to the hydrogel, MSCs do not respond to stiffness in the same manner. MSCs cultured on soft hydrogels behave similar whether HAVDI is present or not. Most cells present a small, round morphology and have mostly cytosolic YAP. However, the presence of HAVDI induces a notable change in MSC behavior on stiff hydrogels. MSCs are small and round, and have mostly cytosolic YAP, similar to levels of MSCs cultured on soft hydrogels. These results indicate that there is competition between cellular matrix mechanosensing and cell-cell signaling to guide MSC behavior.

Understanding how substrate stiffness and cell-cell signaling affect MSC behavior provides a clearer explanation for the results. Stiff substrates increase cytoskeletal tension within MSCs, activating the ROCK signaling pathway and ultimately driving nuclear localization of YAP. The HAVDI peptide is competing with the mechanosensing ability of the MSCs by facilitating cadherin binding and activation of the Hippo pathway, which excludes YAP from the nucleus and limits cellular contractility. The location of YAP within the cell acts as a barometer for researchers to gauge whether stiffness or HAVDI signaling is the predominant force affecting the cells. As seen by increased cytosolic YAP for MSCs cultured on stiff hydrogels with 2 mM HAVDI, cell-cell signaling overpowered the mechanosensing ability of the cell. The effects of HAVDI physically manifested by directing cells to have a smaller cell area and a round morphology, which are contradictory behaviors to MSCs on stiff substrates. Small area and round morphology are both characteristic traits of MSCs cultured on soft hydrogels. This

explains why MSCs grown on soft hydrogels were not significantly different whether HAVDI was present or not, and this was further observed with no significant change in nuclear YAP localization between HAV(-) and HAV(+) groups.

A similar trend is observed when MSCs are cultured on dynamic hydrogels, where the stiffness is increased in the presence of cells. When HAVDI is not present, most cells adapt to the stiff substrate and display a large, spread cellular and nuclear morphology and more nuclear YAP. When HAVDI is coupled to the hydrogels, fewer cells adapted to the stiffened environment, displaying a smaller and rounder nuclear and cellular morphology and more cytoplasmic YAP. These results suggest that cell-cell signaling not only affects MSCs ability to mechanosense on a static substrate, but also its ability to adapt to a new substrate. Cells are known to store information and be influenced by the mechanical stimuli of previous substrates. This is critically important in understanding the issue of mechanical dosing that occurs when MSCs are expanded on TCP, which is orders of magnitude stiffer than native tissue. Obtaining a greater control over the ability of MSCs to be influenced by substrate stiffness can lead toward greater control over mechanical bias caused by TCP.

Chapter 4

NorHA Hydrogel to Evaluate Varying HAVDI Concentrations on MSCs

4.1 Overview

The NorHA macromer allowed for simple conjugation of peptides during or after hydrogel formation via photoinitiated bonds forming between norbornene and a thiol group on peptides [22]. Altering peptide concentration was significantly easier using NorHA hydrogels than pre-coupling process that was required for MeHA hydrogels. Therefore, NorHA hydrogels were used to evaluate the effect of various HAVDI concentrations on MSC behavior. In Chapter 3, the results demonstrated that 2 mM HAVDI impacts cell area, morphology, and mechanosensing on stiff and dynamic hydrogels. Using the NorHA hydrogel system, three HAVDI concentrations were examined to understand how HAVDI affects MSCs cultured on different substrates: 0 mM, 0.5 mM, and 1 mM HAVDI. These values were chosen to determine if a lower concentration of HAVDI will affect MSCs similarly to 2 mM HAVDI, which was evaluated in Chapter 3.

4.2 Materials and Methods

4.2.1 MSC Culture

Bone marrow derived MSCs were purchased from Lonza and reached a passage number between P2 and P5 prior to seeding. MSCs were stored in liquid nitrogen at a cell density of 500,000 cells/vial. Cells were thawed and expanded on TCP dishes prior to experimentation. MSCs were cultured with alpha minimum essential media containing

streptomycin, penicillin, and 10% fetal bovine serum (FBS). Cells were expanded until 80%-90% confluency before passaging or seeding. When the cells reached the desired confluency, they were washed with PBS and then incubated with trypsin for 5 minutes to facilitate cellular detachment from the TCP. Media was then added to the cells to offset the effects of the trypsin. The MSCs, media, and trypsin were combined in a conical tube and centrifuged at 500g for 5 minutes. The supernatant was then removed, and the remaining cell pellet was resuspended in media. The cells were counted using a hemacytometer and then seeded on hydrogels, passaged to a new petri dish, or refrozen in liquid nitrogen.

4.2.2 MSC Staining

After the MSCs were cultured on hydrogels for a set length of time, they were fixed and stained. The MSCs were fixed by incubating them 10% formalin for 10 minutes. The hydrogels were then washed and a permeabilization solution, consisting of a 1:10 dilution of Triton-X in PBS, was added to each hydrogel for 3 minutes. The MSCs were washed again and then a blocking buffer was added to each hydrogel for 30 minutes. The blocking buffer was created by dissolving 3 wt% bovine serum albumin (BSA) in PBS. While the MSCs were in the blocking buffer, a primary YAP solution was prepared using a 1:200 dilution of mouse IgG YAP antibodies in blocking buffer. After blocking was completed, the primary YAP solution was added to the MSCs, and cells were stored in darkness for 1 hour. The hydrogels were then washed 4 times to remove excess antibodies. During the washing steps, a secondary YAP solution was prepared using a 1:200 dilution of anti-mouse IgG antibodies in blocking buffer. The MSCs were

incubated with the secondary YAP solution after the washing was complete and stored in darkness for 2 hours. The hydrogels were then washed five times and a phalloidin solution was created using a 1:200 dilution of 568 wavelength phalloidin in blocking buffer. The hydrogels were soaked in the phalloidin solution for 15 minutes in and then washed twice. A Hoechst solution was prepared using a 1:2500 dilution of Hoechst in PBS and the solution was added to the MSCs for 5 minutes. The hydrogels were then washed twice, and the well-plate was wrapped in foil and stored in 4 degrees Celsius until imaging.

4.2.3 Imaging and Analysis

Hydrogel surface imaging was conducted on a Confocal Microscope using the 20x objective lens. Cellular analysis was completed using the Fiji is just ImageJ (FIJI) software. The nuclear YAP concentrations of MSCs were calculated in several steps. First, masks of the cytoplasm and nucleus of the cell were created using the phalloidin and Hoechst channels. These masks were placed atop the YAP channel to obtain a nuclear and cellular YAP intensity, and each intensity was normalized to its respective area. The normalized nuclear YAP was then divided by the normalized cellular YAP to obtain a nuclear-to-cellular YAP ratio. In addition to nuclear YAP ratios, cellular and nuclear size and morphology were characterized by separating the phalloidin and Hoechst channels, converting the image to black-and-white, and using FIJI's inherent measuring tools.

4.2.4 Statistical Analysis

Statistical analysis for data comparing two variables, an unpaired t test was used, assuming equal standard deviations. When examining three or more variables, an ANOVA test followed by a post-hoc Tukey test was used,

4.3 Results and Discussion

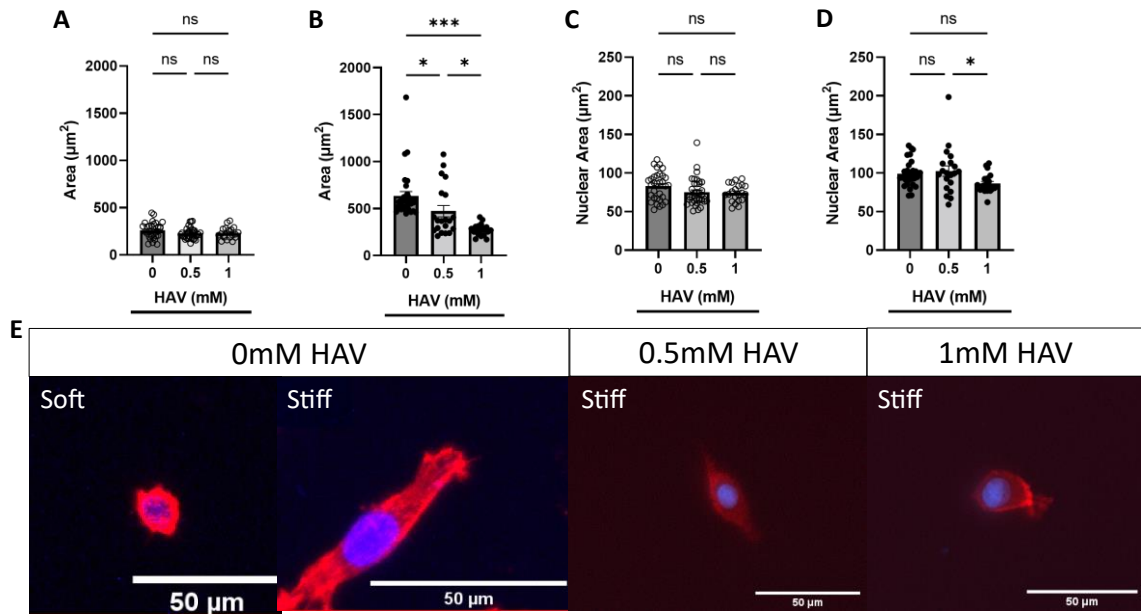
4.3.1 Static MSC Area Analysis on NorHA

When looking at cellular area on soft hydrogels, no significant difference was observed among MSCs cultured on hydrogels with 0 mM, 0.5 mM, or 1mM HAVDI (**Figure 16A**). However, the addition of HAVDI to stiff hydrogels did produce a significant effect on MSC area. The average cellular area of MSCs cultured on stiff hydrogels without HAVDI was $\sim 635.99 \mu\text{m}^2$. When hydrogels contained 0.5 mM HAVDI, the average cellular area decreased to $\sim 472.37 \mu\text{m}^2$. Cell area continued to decrease as HAVDI concentration increased, with the average cellular area reaching $\sim 273.45 \mu\text{m}^2$ when MSCs were cultured on stiff hydrogels with 1 mM HAVDI (**Figure 16B & E**). MSCs cultured on stiff hydrogels with 0 mM HAVDI were significantly larger than MSCs cultured on stiff hydrogels with 0.5 mM or 1 mM HAVDI. Additionally, MSCs cultured on stiff hydrogels with 0.5 mM HAVDI were significantly larger than MSCs cultured on stiff hydrogels with 1 mM HAVDI. Overall, MSC cellular area decreased as HAVDI concentration increased, which suggested that HAVDI concentrations as low as 0.5 mM affected MSC matrix mechanosensing.

The nuclear area of MSCs cultured on soft hydrogels was unaffected by the addition of HAVDI, as no significant difference in nuclear area was observed among hydrogels with 0 mM, 0.5 mM, or 1 mM HAVDI (**Figure 16C**). When MSCs were cultured on stiff hydrogels, no significant difference was observed between MSC cultured on hydrogels with 0 mM or 0.5 mM HAVDI. However, the nuclei of MSCs cultured on stiff hydrogels with 1 mM HAVDI were significantly smaller than the nuclei of MSCs cultured on hydrogels with 0.5 mM HAVDI. MSCs cultured on stiff hydrogels with 0.5 mM HAVDI had an average nuclear area $\sim 102.50 \mu\text{m}^2$. MSCs cultured on stiff hydrogels with 1 mM HAVDI had an average nuclear area $\sim 86.34 \mu\text{m}^2$ (**Figure 16D**). Nuclear area only decreased when MSCs were cultured on hydrogels with 1 mM HAVDI, which suggested that MSC nuclear area was less sensitive to HAVDI and concentrations less than 1 mM HAVDI did not affect the nuclear morphology.

Figure 16

Cellular and Nuclear Area of MSCs on Static NorHA Hydrogels



Note. Cellular area of MSCs cultured on (A) soft and (B) stiff NorHA hydrogels with 0 mM, 0.5 mM, and 1 mM HAVDI. Nuclear area of MSCs cultured on (C) soft and (D) stiff NorHA hydrogels with 0 mM, 0.5 mM, and 1 mM HAVDI. (E) Representative images of MSCs (red, actin; blue, nuclei) cultured on soft hydrogels with 0 mM and stiff hydrogels with 0 mM, 0.5 mM, and 1 mM HAVDI. Bar graphs represent the mean and points individual cells; ns, not significant, * $p < 0.05$, *** $p < 0.001$.

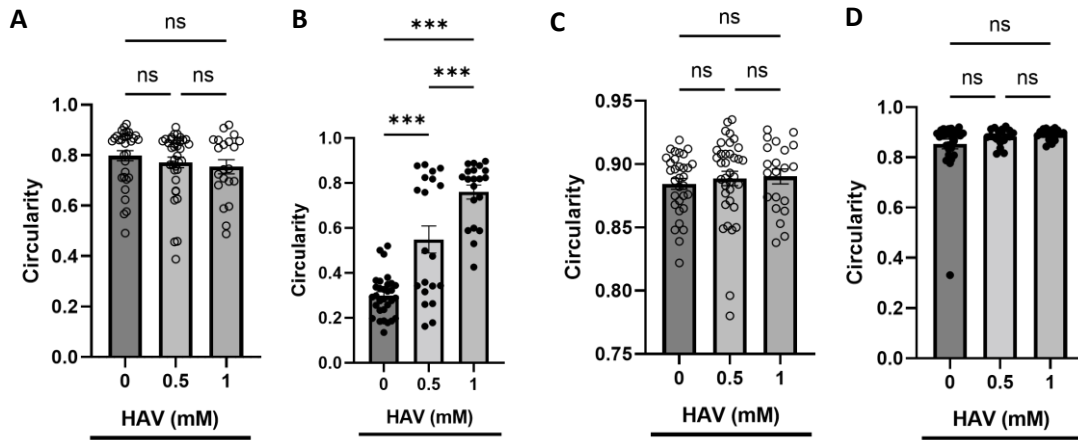
4.3.2 Static MSC Morphology Analysis on NorHA

When looking MSCs cultured on soft hydrogels, no significant difference in cellular circularity was observed among hydrogels cultured on soft hydrogels with 0 mM, 0.5 mM, or 1 mM HAVDI (Figure 17A). However, cellular circularity was impacted by HAVDI concentration when MSCs were cultured on stiff hydrogels. The average cellular circularity of MSCs cultured on stiff hydrogels without HAVDI was ~0.30. When hydrogels contained 0.5 mM HAVDI, the average cellular circularity rose to ~0.55. Cell

circularity continued to increase as HAVDI concentration increased, with the average cellular circularity reaching ~0.76 when MSCs were cultured on stiff hydrogels with 1 mM HAVDI (**Figure 17B**). MSCs cultured on stiff hydrogels with 0 mM HAVDI were significantly less circular than MSCs cultured on stiff hydrogels with 0.5 mM or 1 mM HAVDI. Additionally, MSCs cultured on stiff hydrogels with 0.5 mM HAVDI were significantly less circular than MSCs cultured on stiff hydrogels with 1 mM HAVDI. The direct correlation between circularity and HAVDI concentration further demonstrated that low concentrations of HAVDI are sufficient to drive changes in MSC phenotype. Unlike the cellular circularity, MSC nuclear circularity was not significantly affected by 0 mM, 0.5 mM, or 1 mM HAVDI concentrations on soft or stiff hydrogels (**Figure 17C & D**).

Figure 17

Cellular and Nuclear Circularity of MSCs on Static NorHA Hydrogels



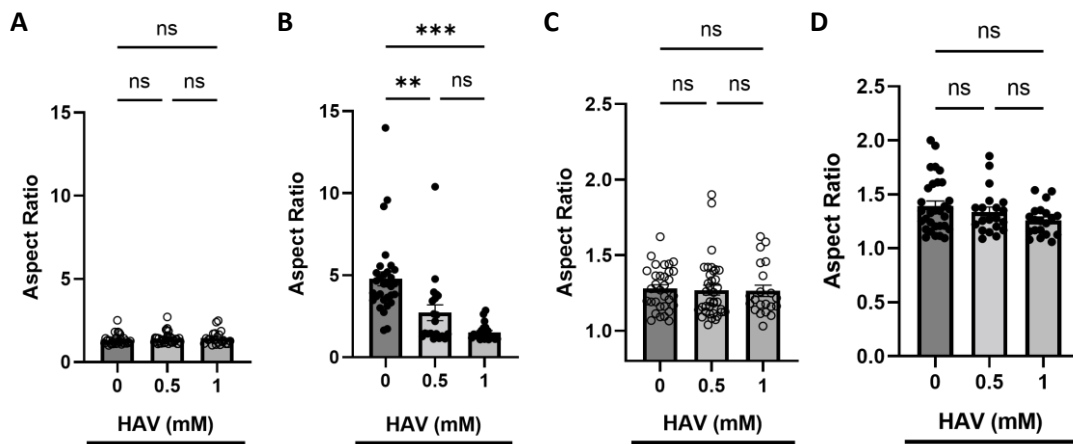
Note. Cellular circularity of MSCs cultured on (A) soft and (B) stiff NorHA hydrogels with 0 mM, 0.5 mM, and 1 mM HAVDI. Nuclear circularity of MSCs cultured on (C) soft and (D) stiff NorHA hydrogels with 0 mM, 0.5 mM, or 1 mM HAVDI. Bar graphs represent the mean and points individual cells; ns, not significant, *** $p < 0.001$.

MSC cellular aspect ratio was not significantly affected by varying HAVDI concentrations on soft hydrogels (**Figure 18A**). When MSCs were cultured on stiff hydrogels, cellular aspect ratio was impacted by HAVDI concentration. The average cellular aspect ratio of MSCs cultured on stiff hydrogels without HAVDI was ~ 4.78 . When hydrogels contained 0.5 mM HAVDI, the average cellular aspect ratio dropped to ~ 2.72 . Cell aspect ratio continued to decrease as HAVDI concentration increased, with the average cellular circularity reaching ~ 1.51 when MSCs were cultured on stiff hydrogels with 1 mM HAVDI (**Figure 18B**). The cellular aspect ratio of MSCs cultured on stiff hydrogels with 0 mM HAVDI was significantly greater the aspect ratio of MSCs cultured on stiff hydrogels with 0.5 mM or 1 mM HAVDI. As the concentration of

HAVDI increased, the cellular aspect ratio decreased, which indicates that HAVDI guided MSCs towards a small, round morphology. This trend was also observed within cellular area and cellular circularity data. The data suggested that small concentrations of HAVDI are adequate to prompt physical changes in the cell. MSC nuclear aspect ratio was not significantly different among soft or stiff hydrogels with 0 mM, 0.5 mM, or 1 mM HAVDI (Figure 18C & D).

Figure 18

Cellular and Nuclear Aspect Ratio of MSCs on Static NorHA Hydrogels



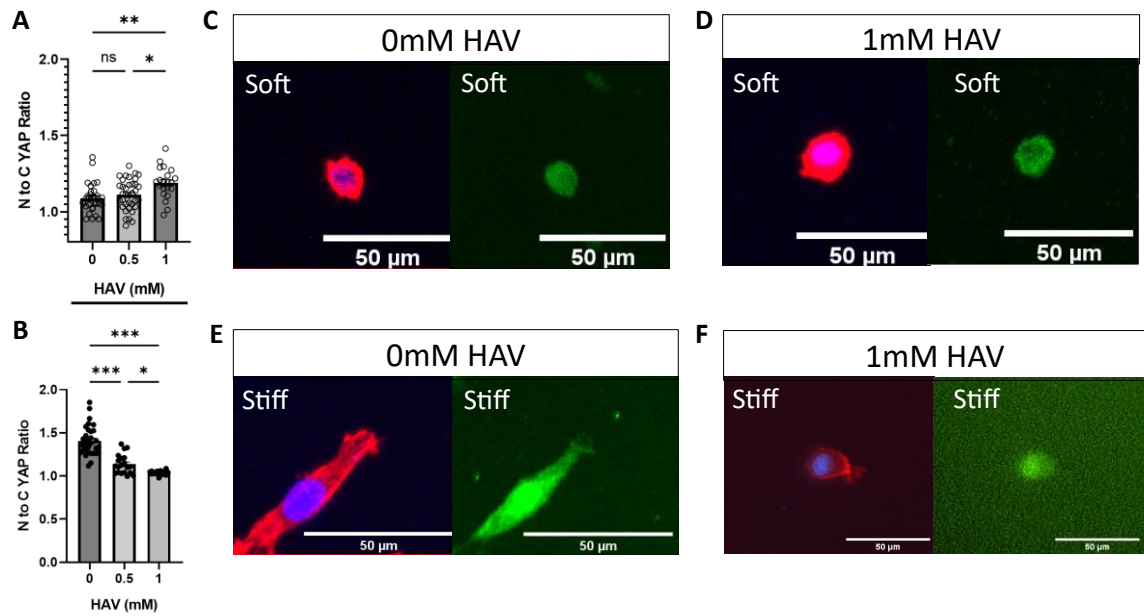
Note. Cellular aspect ratio of MSCs cultured on (A) soft and (B) stiff NorHA hydrogels with 0 mM, 0.5 mM, and 1 mM HAVDI. Nuclear aspect ratio of MSCs cultured on (C) soft and (D) stiff NorHA hydrogels with 0 mM, 0.5 mM, or 1 mM HAVDI. Bar graphs represent the mean and points individual cells; ns, not significant, ** $p < 0.01$, *** $p < 0.001$.

4.3.3 Static MSC Nuclear YAP Analysis on NorHA

When MSCs were cultured on soft NorHA hydrogels, no significant difference in nuclear YAP ratio was observed between hydrogels containing 0 mM or 0.5 mM HAVDI. However, the nuclear YAP of MSCs cultured on hydrogels with 1mM HAVDI was significantly greater than the nuclear YAP of MSCs cultured on hydrogels with 0 mM or 0.5 mM HAVDI (**Figure 19A, C & D**). This result is likely an outlier and due to small sample size because soft hydrogels and the presence of HAVDI have both proven to reduce nuclear YAP localization. Additionally, nuclear YAP is difficult to quantify for small cells with nuclear area being a comparable size to cellular area, which could possibly explain the outlier result. When MSCs were cultured on stiff hydrogels, nuclear YAP was impacted by HAVDI. When MSCs were cultured on stiff hydrogels with 0 mM HAVDI, the nuclear YAP ratio was ~1.41. When the HAVDI concentration increased to 0.5 mM, the nuclear YAP ratio was ~1.14. As the HAVDI concentration further increased to 1 mM, the nuclear YAP ratio fell to ~1.04 (**Figure 19B, E & F**). The differences in nuclear YAP among hydrogels with 0 mM, 0.5 mM, and 1 mM HAVDI were statistically significant. The nuclear YAP data, along with the size and morphology data, suggests that HAVDI inhibits MSC matrix mechanosensing with concentrations as low as 0.5 mM.

Figure 19

Nuclear YAP of MSCs Cultured on Static NorHA Hydrogels



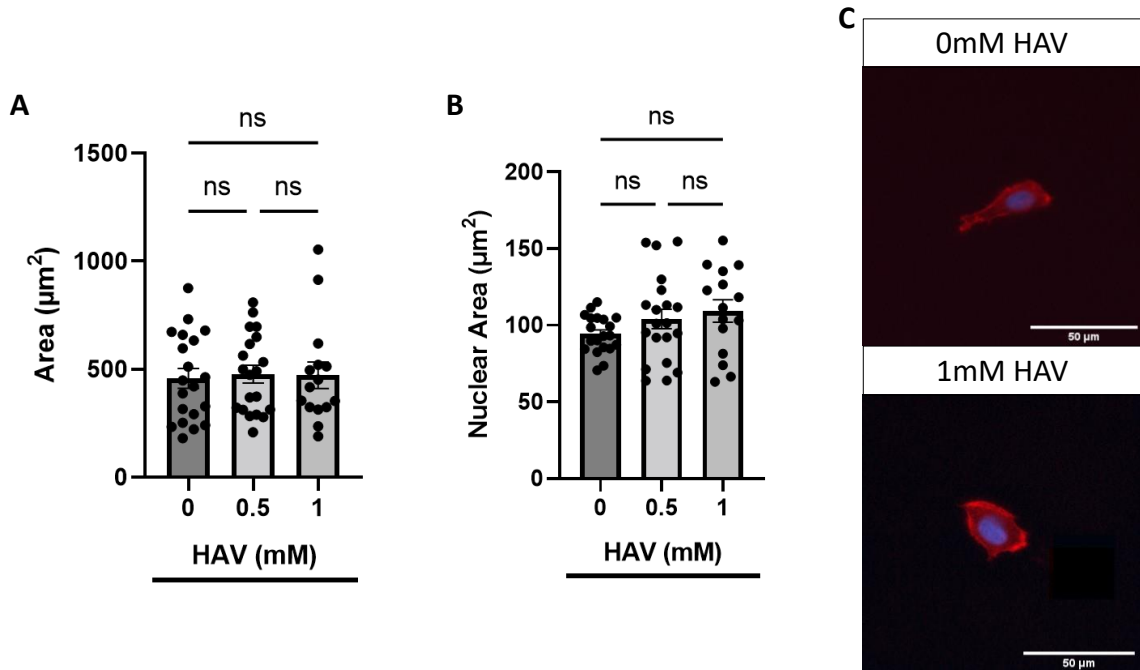
Note. Nuclear to cytoplasmic YAP ratios of MSCs cultured on (A) soft and (B) stiff NorHA hydrogels with 0 mM, 0.5 mM, or 1 mM HAVDI. Representative images of MSCs (red, actin; blue, nuclei; green, YAP) cultured on (C) soft hydrogels with 0 mM HAVDI, (D) soft hydrogels with 1 mM HAVDI, (E) stiff hydrogels with 0 mM HAVDI, and (F) stiff hydrogels with 1 mM HAVDI. Bar graphs represent the mean and points individual cells; ns, not significant, * $p < 0.05$, ** $p < 0.01$, *** $p < 0.001$.

4.3.4 Dynamic MSC Area Analysis on NorHA

Despite the difference in cellular area observed on stiff static hydrogels, no significant difference in cellular area was observed among dynamic hydrogels with 0 mM, 0.5 mM, and 1 mM HAVDI (Figures 20A & C). MSC nuclear area was also not significantly affected by different concentrations of HAVDI (Figures 20B & C). These results suggest that HAVDI effects mechanosensing and mechanoadaptation differently, with mechanosensing pathways being more sensitive to lower concentration of HAVDI.

Figure 20

Cellular and Nuclear Area of MSCs on Dynamic NorHA Hydrogels



Note. (A) Cellular and (B) nuclear area quantification of MSCs cultured on dynamic (in situ) NorHA hydrogels with 0 mM, 0.5 mM, or 1 mM HAVDI. (C) Representative images of MSCs (red, actin; blue, nuclei) cultured on dynamic hydrogels with 0 mM or 1 mM HAVDI. Bar graphs represent the mean and points individual cells; ns, not significant.

4.3.5 Dynamic MSC Morphology Analysis on NorHA

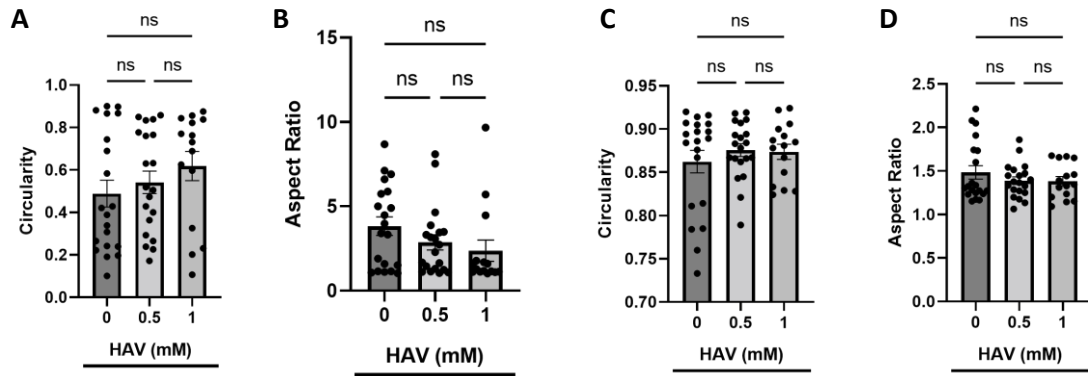
When MSCs were cultured on stiffened hydrogels, no significant difference in cellular circularity was observed among hydrogels containing 0 mM, 0.5 mM, and 1 mM HAVDI. Despite the lack of statistical significance among HAVDI concentration, the average cellular circularity increased as HAVDI concentration increased. MSCs cultured on stiffened hydrogels with 0 mM HAVDI had an average cellular circularity ~ 0.49 . The average cellular circularity increased to ~ 0.54 when MSCs were cultured on dynamic

hydrogels with 0.5 mM HAVDI. MSC average cellular circularity continued to increase to ~0.62 when MSCs were cultured on dynamic hydrogels with 1 mM HAVDI (**Figure 21A**). The relationship between cell circularity and HAVDI concentration led me to believe that HAVDI influences the mechanoadaptation ability of MSCs, but higher concentrations that 1 mM are required to achieve a significant difference. There was no significant difference in nuclear circularity between MSCs cultured on dynamic hydrogels with 0 mM, 0.5 mM, or 1 mM HAVDI (**Figure 21C**).

When MSCs were cultured on stiffened hydrogels, no significant difference in cellular aspect ratio was observed among hydrogels containing 0 mM, 0.5 mM, and 1 mM HAVDI. Despite the lack of statistical significance among HAVDI concentration, the average cellular aspect ratio decreased as HAVDI concentration increased. MSCs cultured on stiffened hydrogels with 0mM HAVDI had an average cellular aspect ratio ~3.83. The average cellular aspect ratio decreased to ~2.87 when MSCs were cultured on dynamic hydrogels with 0.5 mM HAVDI. MSC average cellular aspect ratio further decreased to ~2.38 when MSCs were cultured on dynamic hydrogels with 1 mM HAVDI (**Figure 21B**). MSC cellular aspect ratio data further suggests that HAVDI has an impact on MSC mechanoadaptation, but also indicates that concentration greater than 1 mM are required to achieve a significant difference in cell morphology. There was no significant difference in nuclear aspect ratio between MSCs cultured on dynamic hydrogels with 0 mM, 0.5 mM, or 1 mM HAVDI (**Figure 21D**).

Figure 21

Cellular and Nuclear Morphology of MSCs on Dynamic NorHA Hydrogels



Note. Cellular (A) circularity and (B) aspect ratio of MSCs cultured on dynamic (in situ) NorHA hydrogels with 0 mM, 0.5 mM, or 1 mM HAVDI. Nuclear (C) circularity and (D) aspect ratio of MSCs cultured on dynamic NorHA hydrogels with 0 mM, 0.5 mM, or 2 mM HAVDI. Bar graphs represent the mean and points individual cells; ns, not significant.

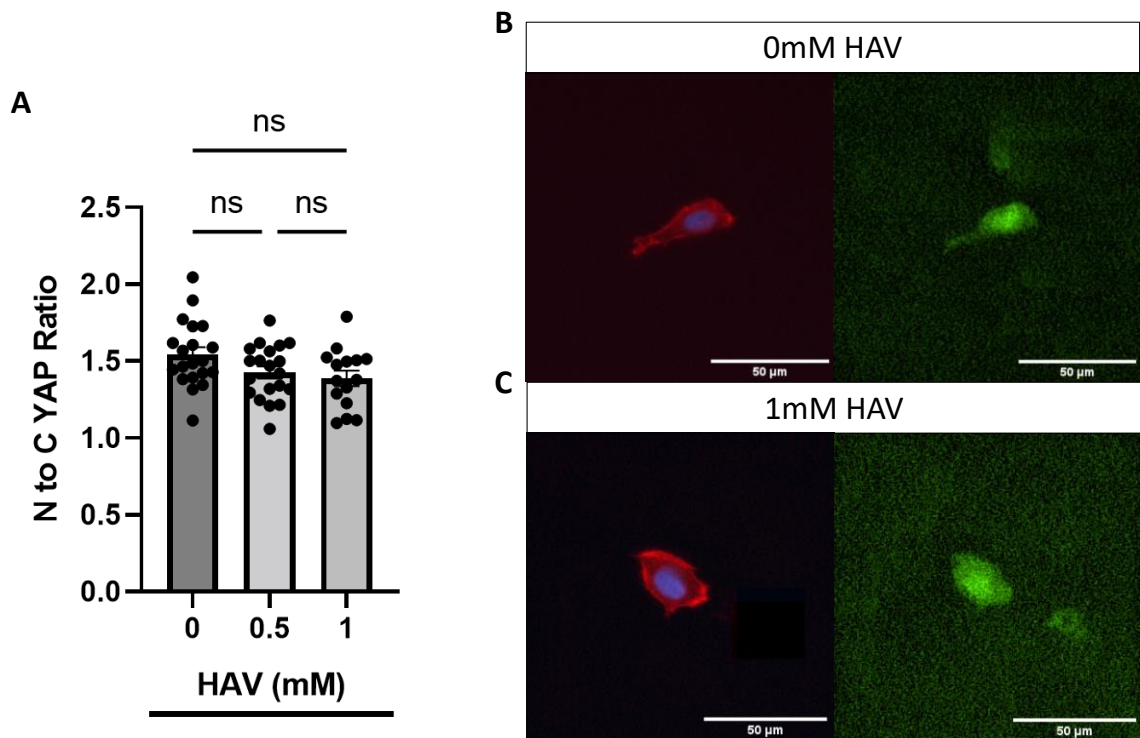
4.3.6 Dynamic MSC Nuclear YAP Analysis on NorHA

When MSCs were cultured on dynamic NorHA hydrogels, no significant difference in nuclear YAP ratios were observed among MSCs containing 0 mM, 0.5 mM, or 1 mM HAVDI. Despite the lack of statistical significance, a decrease in nuclear YAP was observed as HAVDI concentration increased. MSCs cultured on stiffened hydrogels with 0 mM HAVDI had an average nuclear YAP \sim 1.54. The nuclear YAP concentration decreased to \sim 1.43 when MSCs were cultured on dynamic hydrogels with 0.5 mM HAVDI. MSC nuclear YAP concentrations further decreased to 1.39 when MSCs were cultured on dynamic hydrogels with 1 mM HAVDI (Figure 22A-C). The trend in nuclear YAP ratio reinforced the tendencies observed in cellular morphology data. HAVDI does

impact MSC mechanosensing, but concentration greater than 1 mM are necessary to see a significant difference.

Figure 22

Nuclear YAP of MSCs Cultured on Dynamic NorHA Hydrogels



Note. (A) Nuclear to cytoplasmic YAP ratios of MSCs cultured on dynamic (in situ) NorHA hydrogels with 0 mM, 0.5 mM, or 1 mM HAVDI. Representative images of MSCs (red, actin; blue, nuclei; green, YAP) cultured on dynamic hydrogels with (B) 0 mM HAVDI and (C) 1 mM HAVDI. Bar graphs represent the mean and points individual cells; ns, not significant.

4.4 Conclusion

Utilizing the NorHA hydrogel system allowed for greater control over the concentration of peptides presented than the MeHA hydrogel system. NorHA was used to evaluate the effect that 0 mM, 0.5 mM, and 1 mM HAVDI had on MSC behavior. When MSCs were cultured on static hydrogels without HAVDI, hydrogel stiffness continued to dictate MSC behavior. MSCs cultured on soft hydrogels had a small, round morphology and cytosolic YAP. MSCs cultured on stiff hydrogels had a large, spread morphology and nuclear YAP. When HAVDI was coupled to the hydrogels, MSCs did not adhere to the same trend. When MSCs were cultured on soft hydrogels, the cells remained small and round, independent of HAVDI concentration. However, there appeared to be a positive correlation between nuclear YAP and HAVDI concentration. This result is likely due to a low sample size ($n \geq 21$) and difficulty quantifying nuclear YAP in smaller cells. When HAVDI was introduced to stiff hydrogels, even at concentrations as low as 0.5mM, drastic changes in cell behavior were observed. As HAVDI concentration increased, MSCs adopted a smaller and rounder morphology. Additionally, nuclear YAP significantly decreased as HAVDI concentration increased. These results suggest that cell-cell signaling is a potent regulator of nuclear YAP localization, and that small concentration are sufficient to overcome signals from cellular mechanosensing.

Despite the significant impact that HAVDI had on MSCs in a static environment, HAVDI appeared to be less impactful at influencing MSC mechanoadaptation. There appeared to be no correlation between HAVDI concentration and cell area for MSCs cultured on dynamic hydrogels. Additionally, no significant difference in cell

morphology or nuclear YAP ratio was observed between MSCs cultured on dynamic substrates with varying HAVDI concentrations. Despite the lack of significance, HAVDI concentration appeared to be directly correlated to a small, round cellular morphology and decreased nuclear YAP. This suggests that low concentrations of HAVDI impact the mechanoadaptation ability of MSCs, however concentration greater than 1mM are required to achieve a significant difference. Overall, the results from chapters 3 and 4 indicated that cell-cell signaling is a powerful regulator of MSC mechanosensing and mechanoadaptation, and that concentrations as low as 0.5mM influenced cell behavior.

Chapter 5

Summary and Future Directions

5.1 Summary

Examining how cells behave in vitro could help explain why HAVDI affects matrix mechanosensing on different substrates. Nuclear localization of YAP causes downstream signaling resulting in cell growth and inactivation of apoptotic genes. At a low density, cells grow and proliferate until they eventually become confluent and are capable of forming adherens junctions with adjacent cells. Once reaching a high confluency, cells no longer have the available space to continue growing and may begin competing for limited resources. This is where cell-cell signaling is activated. N-cadherin-mediated cell-cell signaling activate the Hippo pathway which ultimately results in YAP exclusion from the nucleus. Without nuclear YAP, cells are no longer instructed to grow, like cells cultured on soft substrates. Although substrate stiffness and cell-cell signaling are upstream regulators of different biological pathways, both stimuli share a common downstream effect, YAP localization within the cell. The competitive behavior between matrix mechanosensing and cell-cell signaling drives that difference in cell behavior on stiff hydrogels when HAVDI is present.

To further advance the knowledge obtained in this work, a few limitations must be overcome. The established hydrogel systems are effective in studying the effects of cell-cell signaling on MSC mechanoadaptation but fail to consider the consequence of mechanical dosing on the mechanical memory of MSCs. Given the role of HAVDI in

reducing MSCs mechanosensing and mechanoadaptation ability, we hypothesize that HAVDI will reduce the effect of mechanical dosing on stiff environments. The influence of HAVDI on mechanical memory could easily be studied by slightly modifying the established hydrogel systems. MSCs could be mechanically dosed on stiff hydrogels with photodegradable crosslinkers, that can be degraded on demand, in the presence of HADVI (**Section 5.2**). Additionally, the established hydrogel systems aspire to mimic natural tissue more accurately than static biomaterials but fail to address the 3-dimensional aspect of native tissue. Therefore, the established NorHA hydrogel system containing HAVDI could be adapted to encapsulate MSCs and evaluate mechanosensing in a more physiologically accurate environment (**Section 5.3**).

5.2 Effect of Mechanical Dosing on MSCs

It has been well documented that MSCs are able to retain mechanical information from previous environments they have been cultured on. Using this knowledge, it follows that expanding MSCs on TCP, which is much stiffer than any native tissue, creates a mechanical bias that influences cell behavior. MSCs grown on stiff substrates tend to favor osteogenic differentiation, which is problematic if other MSC lineages are desired.

Building off the concept of mechanical dosing, an interesting follow up study could examine the effect of dosing MSCs on stiff hydrogels containing HAVDI and then softening the hydrogels. The established NorHA hydrogel system could be used to create a dynamic softening approach, following an approach similar to the one outlined by Rosales et al [72]. The stiff hydrogels could be created using photocleavable crosslinks. After a period of mechanical dosing, the hydrogel could be exposed to ultraviolet light

and some of the crosslinks would be removed, decreasing the elastic modulus of the hydrogel. To further isolate the effect of mechanical dosing on stiff hydrogels, MSCs could be isolated directly from bone marrow and expanded on substrates softer than TCP. One option for MSC expansion is hydrogel coated petri dishes, called PetriSoft, which can be purchased from a company called Matrigen. The PetriSoft dishes are available in a variety of stiffnesses and can even be ordered with a custom stiffness. Ideally, PetriSoft dishes with lowest stiffness that still promote cell proliferation would be used to expand the cells prior to seeding them on stiff hydrogels with and without HAVDI.

5.2.1 NorHA Hydrogel System to Evaluate the Effect of Mechanical Dosing

Prior to beginning experiments, MSCs must be isolated from bone marrow. Once MSCs have been obtained, they must be assessed using flow cytometry to verify that MSC specific surface markers are present on the cells and white blood cell markers are not present on the cells. After confirming that the collected cells are MSCs, experimentation can begin. MSCs should be expanded on PetriSoft dishes until a desired confluency is achieved. All hydrogels will contain 2mM RGD and HAVDI concentration will vary between 0mM and 2mM.

5.2.2 Preliminary Results

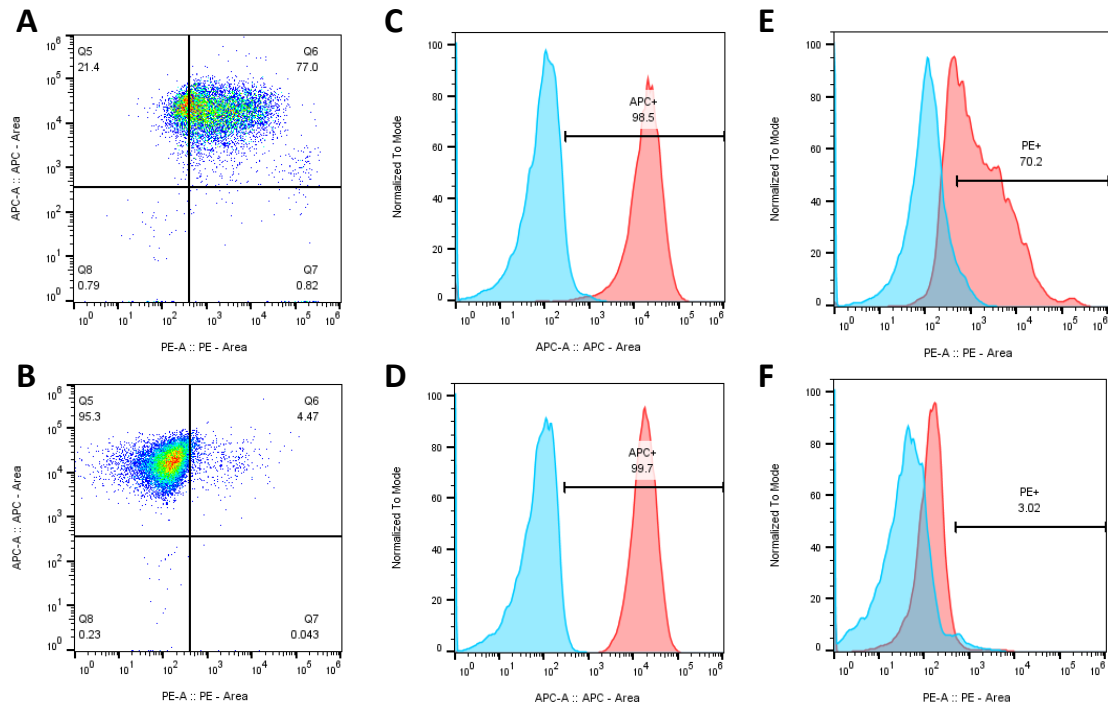
MSCs were isolated from bone marrow and cultured directly on 2 kPa and 8 kPa PetriSoft dishes to determine if those stiffnesses were sufficient to promote cell growth. A brightfield microscope was used to track the development of MSCs expanded on both hydrogel-coated dishes. After 10 days, which was the maximum number of days examined using the microscope, MSCs did not appear to grow or proliferate on the 2 kPa

PetriSoft dish. MSCs expanded on the 8 kPa PetriSoft dish appeared to grow slightly more than MSCs on the 2 kPa PetriSoft dish, but proliferation was also halted within 10 days as well. The lack of growth and proliferation of MSCs suggests that PetriSoft dishes with greater stiffnesses are required for MSC expansion.

Flow cytometry of MSCs derived from bone marrow was also conducted to confirm that MSC surface markers were present on the collected cells. Due to the lack of proliferation of MSCs grown on 2 kPa and 8kPa PetriSoft, the bone marrow derived MSCs were expanded on TCP. MSCs that had undergone 2 passages (P2) highly expressed MSC surface markers and the negative cocktail, which stained primarily for white blood cell surface markers (**Figure 23A, C & E**). MSCs that had experienced 5 passages (P5) continued to highly express MSC surface markers, but the negative cocktail expression decreased (**Figure 23B, D & F**). We hypothesize that low passage MSCs highly expressed the negative cocktail because white blood cells from the bone marrow were collected with the stem cells. As MSCs experienced more passaging, the white blood cells should be washed away, corresponding to the decrease in negative cocktail expression.

Figure 23

Flow Cytometry of High and Low Passage MSCs



Note. CD90 MSC surface marker expression versus negative cocktail expression of (A) P2 and (B) P5 MSCs. CD90 MSC surface marker expression of (C) P2 and (D) P5 MSCs. Negative cocktail expression of (E) P2 and (F) P5 MSCs.

5.3 Effect of Engineered Cell-Cell Signaling on MSC Remodeling in 3D

5.3.1 MSC Behavior Encapsulated within 3D Hydrogels

Just as dynamic hydrogel systems more accurately mimic human tissue, 3-dimensional hydrogels that can encapsulate cells are a more accurate representation of native tissue than 2-dimensional hydrogels. MSCs encapsulated within 3D hydrogels behave differently than MSCs cultured atop 2D hydrogels. In 2D, hydrogel stiffness has a significant effect on MSC behavior, with stiff hydrogels corresponding to high nuclear

YAP and a large, spread morphology. In 3D, stiffness appears to have an inverse effect, with stiff hydrogels corresponding to low nuclear YAP and a small, round morphology [11]. More important than hydrogel stiffness is the ability of MSCs to remodel their surroundings. When MSCs were encapsulated within a hydrogel with degradable crosslinkers, cell spreading and nuclear YAP increased compared to a hydrogel of the same stiffness with a nondegradable crosslinker [11]. Coupling HAVDI peptides to the hydrogel system to mimic cell-cell signaling may impact the ability of MSCs to remodel their surroundings.

5.3.2 Theoretical Effect of Cell-Cell Signaling on MSC Matrix Remodeling

NorHA hydrogels have already been used for 3D studies, so the established NorHA hydrogel system could be slightly modified for encapsulating MSCs [11, 73, 74]. Rather than comparing hydrogels with different stiffnesses, a single stiffness could be used and the degradability of the crosslinker could be varied. All hydrogels could contain a total peptide concentration of 4mM, with each hydrogel containing 2mM RGD. Hydrogels will contain 0mM, 1mM, or 2mM HAVDI, with scrambled HAVDI added to achieve 4mM total peptide concentration, when necessary. For cells to achieve nuclear localized YAP in 3D, they must be able to remodel their environment and generate cytoskeletal tension. When the hydrogel crosslinkers are degradable and HAVDI is not present, microenvironment remodeling can occur [11]. MSCs encapsulated inside hydrogels with degradable crosslinkers should have high nuclear YAP, and MSCs encapsulated with hydrogels with nondegradable crosslinkers should have high cytosolic YAP. As seen in the 2D studies within this paper, cell-cell signaling reduces MSCs ability to generate a

contractile force by activating the Hippo pathway to exclude YAP from the nucleus. Therefore, when MSCs are encapsulated within hydrogels containing HAVDI, a positive correlation should exist between HAVDI concentration and cytosolic YAP, regardless of crosslinker degradability. The combination of RGD and HAVDI coupled 3D hydrogels has proven to be effective in promoting chondrogenic differentiation [73], but the effect of HAVDI on MSC mechanosensing in 3 dimensions has not been explored in depth. Utilizing the 3D NorHA system allows unique biochemical combinations, such as RGD and HAVDI coupling, to be explored in a system that more accurately mimics the natural body.

References

1. Zakrzewski, W., et al., *Stem cells: past, present, and future*. Stem Cell Res Ther, 2019. **10**(1): p. 68.
2. Chagastelles, P.C. and N.B. Nardi, *Biology of stem cells: an overview*. Kidney International Supplements, 2011. **1**(3): p. 63-67.
3. Vojnits, K. and S. Bremer, *Challenges of using pluripotent stem cells for safety assessments of substances*. Toxicology, 2010. **270**(1): p. 10-17.
4. Yoshihara, M., Y. Hayashizaki, and Y. Murakawa, *Genomic Instability of iPSCs: Challenges Towards Their Clinical Applications*. Stem Cell Reviews and Reports, 2017. **13**(1): p. 7-16.
5. Rodriguez, A.M., et al., *The human adipose tissue is a source of multipotent stem cells*. Biochimie, 2005. **87**(1): p. 125-128.
6. Thirumala, S., W.S. Goebel, and E.J. Woods, *Clinical grade adult stem cell banking*. Organogenesis, 2009. **5**(3): p. 143-154.
7. Dominici, M., et al., *Minimal criteria for defining multipotent mesenchymal stromal cells. The International Society for Cellular Therapy position statement*. Cytotherapy, 2006. **8**(4): p. 315-317.
8. Naji, A., et al., *Biological functions of mesenchymal stem cells and clinical implications*. Cellular and Molecular Life Sciences, 2019. **76**(17): p. 3323-3348.
9. Mohamed-Ahmed, S., et al., *Adipose-derived and bone marrow mesenchymal stem cells: a donor-matched comparison*. Stem Cell Research & Therapy, 2018. **9**(1): p. 168.
10. Heathman, T.R.J., et al., *Characterization of human mesenchymal stem cells from multiple donors and the implications for large scale bioprocess development*. Biochemical Engineering Journal, 2016. **108**: p. 14-23.

11. Caliari, S.R., et al., *Dimensionality and spreading influence MSC YAP/TAZ signaling in hydrogel environments*. *Biomaterials*, 2016. **103**: p. 314-323.
12. McBeath, R., et al., *Cell Shape, Cytoskeletal Tension, and RhoA Regulate Stem Cell Lineage Commitment*. *Developmental Cell*, 2004. **6**(4): p. 483-495.
13. Engler, A.J., et al., *Matrix Elasticity Directs Stem Cell Lineage Specification*. *Cell*, 2006. **126**(4): p. 677-689.
14. Wen, J.H., et al., *Interplay of matrix stiffness and protein tethering in stem cell differentiation*. *Nature Materials*, 2014. **13**(10): p. 979-987.
15. Gilbert, P.M., et al., *Substrate Elasticity Regulates Skeletal Muscle Stem Cell Self-Renewal in Culture*. 2010. **329**(5995): p. 1078-1081.
16. Poellmann, M.J., et al., *Geometric microenvironment directs cell morphology on topographically patterned hydrogel substrates*. *Acta Biomaterialia*, 2010. **6**(9): p. 3514-3523.
17. Chaudhuri, O., et al., *Hydrogels with tunable stress relaxation regulate stem cell fate and activity*. *Nature Materials*, 2016. **15**(3): p. 326-334.
18. Dong, J.-d., et al., *Response of mesenchymal stem cells to shear stress in tissue-engineered vascular grafts*. *Acta Pharmacologica Sinica*, 2009. **30**(5): p. 530-536.
19. Rodrigues, M., L.G. Griffith, and A. Wells, *Growth factor regulation of proliferation and survival of multipotential stromal cells*. *Stem Cell Research & Therapy*, 2010. **1**(4): p. 32.
20. Abarbanell, A.M., et al., *Proinflammatory Cytokine Effects on Mesenchymal Stem Cell Therapy for the Ischemic Heart*. *The Annals of Thoracic Surgery*, 2009. **88**(3): p. 1036-1043.
21. Ling, L., V. Nurcombe, and S.M. Cool, *Wnt signaling controls the fate of mesenchymal stem cells*. *Gene*, 2009. **433**(1): p. 1-7.

22. Cosgrove, B.D., et al., *N-cadherin adhesive interactions modulate matrix mechanosensing and fate commitment of mesenchymal stem cells*. Nature Materials, 2016. **15**(12): p. 1297-1306.
23. Mao, A.S., J.-W. Shin, and D.J. Mooney, *Effects of substrate stiffness and cell-cell contact on mesenchymal stem cell differentiation*. Biomaterials, 2016. **98**: p. 184-191.
24. Grashoff, C., et al., *Measuring mechanical tension across vinculin reveals regulation of focal adhesion dynamics*. Nature, 2010. **466**(7303): p. 263-266.
25. Geiger, B., J.P. Spatz, and A.D. Bershadsky, *Environmental sensing through focal adhesions*. Nature Reviews Molecular Cell Biology, 2009. **10**(1): p. 21-33.
26. Anderson, L.R., T.W. Owens, and M.J. Naylor, *Structural and mechanical functions of integrins*. Biophys Rev, 2014. **6**(2): p. 203-213.
27. Jaalouk, D.E. and J. Lammerding, *Mechanotransduction gone awry*. Nature Reviews Molecular Cell Biology, 2009. **10**(1): p. 63-73.
28. Dupont, S., et al., *Role of YAP/TAZ in mechanotransduction*. Nature, 2011. **474**(7350): p. 179-183.
29. Nardone, G., et al., *YAP regulates cell mechanics by controlling focal adhesion assembly*. Nature Communications, 2017. **8**(1): p. 15321.
30. Darnell, M., L. Gu, and D. Mooney, *RNA-seq reveals diverse effects of substrate stiffness on mesenchymal stem cells*. Biomaterials, 2018. **181**: p. 182-188.
31. Park, J.S., et al., *The effect of matrix stiffness on the differentiation of mesenchymal stem cells in response to TGF- β* . Biomaterials, 2011. **32**(16): p. 3921-3930.
32. Yuan, H., et al., *A newly identified mechanism involved in regulation of human mesenchymal stem cells by fibrous substrate stiffness*. Acta Biomaterialia, 2016. **42**: p. 247-257.

33. Yang, C., et al., *Mechanical memory and dosing influence stem cell fate*. Nature Materials, 2014. **13**(6): p. 645-652.
34. Bonab, M.M., et al., *Aging of mesenchymal stem cell in vitro*. BMC Cell Biology, 2006. **7**(1): p. 14.
35. Guvendiren, M. and J.A. Burdick, *Stiffening hydrogels to probe short- and long-term cellular responses to dynamic mechanics*. Nature Communications, 2012. **3**(1): p. 792.
36. Bhat, S., et al., *Expansion and characterization of bone marrow derived human mesenchymal stromal cells in serum-free conditions*. Scientific Reports, 2021. **11**(1): p. 3403.
37. Hudecki, A., G. Kiryczyński, and M.J. Łos, *Chapter 7 - Biomaterials, Definition, Overview*, in *Stem Cells and Biomaterials for Regenerative Medicine*, M.J. Łos, A. Hudecki, and E. Wiecheć, Editors. 2019, Academic Press. p. 85-98.
38. Marin, E., F. Boschetto, and G. Pezzotti, *Biomaterials and biocompatibility: An historical overview*. Journal of Biomedical Materials Research Part A, 2020. **108**(8): p. 1617-1633.
39. Pilliar, R.M., *Metallic Biomaterials*, in *Biomedical Materials*, R. Narayan, Editor. 2021, Springer International Publishing: Cham. p. 1-47.
40. Prasad, K., et al., *Metallic Biomaterials: Current Challenges and Opportunities*. Materials (Basel), 2017. **10**(8).
41. Punj, S., J. Singh, and K. Singh, *Ceramic biomaterials: Properties, state of the art and future prospectives*. Ceramics International, 2021. **47**(20): p. 28059-28074.
42. Piconi, C. and A.A. Porporati, *Bioinert Ceramics: Zirconia and Alumina*, in *Handbook of Bioceramics and Biocomposites*, I.V. Antoniac, Editor. 2016, Springer International Publishing: Cham. p. 59-89.
43. Sheikh, Z., et al., *Biodegradable Materials for Bone Repair and Tissue Engineering Applications*. Materials, 2015. **8**(9).

44. Kulkarni, S.V., A.C. Nemade, and P.D. Sonawwanay. *An Overview on Metallic and Ceramic Biomaterials. in Recent Advances in Manufacturing Processes and Systems*. 2022. Singapore: Springer Nature Singapore.
45. Ozdil, D. and H.M. Aydin, *Polymers for medical and tissue engineering applications*. 2014. **89**(12): p. 1793-1810.
46. Kohane, D.S. and R. Langer, *Polymeric Biomaterials in Tissue Engineering*. *Pediatric Research*, 2008. **63**(5): p. 487-491.
47. Mandal, A., et al., *Hydrogels in the clinic*. *Bioengineering & Translational Medicine*, 2020. **5**(2): p. e10158.
48. Lu, H.D., et al., *Injectable shear-thinning hydrogels engineered with a self-assembling Dock-and-Lock mechanism*. *Biomaterials*, 2012. **33**(7): p. 2145-2153.
49. Charron, P.N., T.A. Braddish, and R. Floreani, *PVA-gelatin hydrogels formed using combined theta-gel and cryo-gel fabrication techniques*. *Journal of the Mechanical Behavior of Biomedical Materials*, 2019. **92**: p. 90-96.
50. Mironi-Harpaz, I., et al., *Photopolymerization of cell-encapsulating hydrogels: Crosslinking efficiency versus cytotoxicity*. *Acta Biomaterialia*, 2012. **8**(5): p. 1838-1848.
51. Chai, Q., Y. Jiao, and X. Yu, *Hydrogels for Biomedical Applications: Their Characteristics and the Mechanisms behind Them*. *Gels*, 2017. **3**(1).
52. DeForest, C.A., E.A. Sims, and K.S. Anseth, *Peptide-Functionalized Click Hydrogels with Independently Tunable Mechanics and Chemical Functionality for 3D Cell Culture*. *Chemistry of Materials*, 2010. **22**(16): p. 4783-4790.
53. Maître, J.-L. and C.-P. Heisenberg, *Three Functions of Cadherins in Cell Adhesion*. *Current Biology*, 2013. **23**(14): p. R626-R633.
54. Klezovitch, O. and V. Vasioukhin, *Cadherin signaling: keeping cells in touch*. *F1000Res*, 2015. **4**(F1000 Faculty Rev): p. 550.

55. Desai, R., et al., *Monomeric α -catenin links cadherin to the actin cytoskeleton*. Nature Cell Biology, 2013. **15**(3): p. 261-273.
56. Kann, A.P., M. Hung, and R.S. Krauss, *Cell–cell contact and signaling in the muscle stem cell niche*. Current Opinion in Cell Biology, 2021. **73**: p. 78-83.
57. Jeanes, A., C.J. Gottardi, and A.S. Yap, *Cadherins and cancer: how does cadherin dysfunction promote tumor progression?* Oncogene, 2008. **27**(55): p. 6920-6929.
58. Kourtidis, A., et al., *A central role for cadherin signaling in cancer*. Exp Cell Res, 2017. **358**(1): p. 78-85.
59. Watanabe, T., K. Sato, and K. Kaibuchi, *Cadherin-mediated intercellular adhesion and signaling cascades involving small GTPases*. Cold Spring Harb Perspect Biol, 2009. **1**(3): p. a003020.
60. Gumbiner, B.M. and N.-G. Kim, *The Hippo-YAP signaling pathway and contact inhibition of growth*. Journal of Cell Science, 2014. **127**(4): p. 709-717.
61. Kim, N.-G., et al., *E-cadherin mediates contact inhibition of proliferation through Hippo signaling-pathway components*. 2011. **108**(29): p. 11930-11935.
62. Hui, T.Y., et al., *In vitro chondrogenic differentiation of human mesenchymal stem cells in collagen microspheres: Influence of cell seeding density and collagen concentration*. Biomaterials, 2008. **29**(22): p. 3201-3212.
63. Caliri, S.R., et al., *Stiffening hydrogels for investigating the dynamics of hepatic stellate cell mechanotransduction during myofibroblast activation*. Scientific Reports, 2016. **6**(1): p. 21387.
64. Guvendiren, M., et al., *Hydrogels with differential and patterned mechanics to study stiffness-mediated myofibroblastic differentiation of hepatic stellate cells*. Journal of the Mechanical Behavior of Biomedical Materials, 2014. **38**: p. 198-208.

65. Gramlich, W.M., I.L. Kim, and J.A. Burdick, *Synthesis and orthogonal photopatterning of hyaluronic acid hydrogels with thiol-norbornene chemistry*. *Biomaterials*, 2013. **34**(38): p. 9803-9811.
66. Zhang, J. and C.A. Reinhart-King, *Targeting Tissue Stiffness in Metastasis: Mechanomedicine Improves Cancer Therapy*. *Cancer Cell*, 2020. **37**(6): p. 754-755.
67. Wells, R.G., *Tissue mechanics and fibrosis*. *Biochim Biophys Acta*, 2013. **1832**(7): p. 884-90.
68. Kohn, J.C., M.C. Lampi, and C.A. Reinhart-King, *Age-related vascular stiffening: causes and consequences*. 2015. **6**.
69. Abatangelo, G., et al., *Hyaluronic Acid: Redefining Its Role*. *Cells*, 2020. **9**(7): p. 1743.
70. Burdick, J.A., et al., *Controlled Degradation and Mechanical Behavior of Photopolymerized Hyaluronic Acid Networks*. *Biomacromolecules*, 2005. **6**(1): p. 386-391.
71. Schuurmans, C.C.L., et al., *Hyaluronic acid and chondroitin sulfate (meth)acrylate-based hydrogels for tissue engineering: Synthesis, characteristics and pre-clinical evaluation*. *Biomaterials*, 2021. **268**: p. 120602.
72. Rosales, A.M., et al., *Hydrogels with Reversible Mechanics to Probe Dynamic Cell Microenvironments*. 2017. **56**(40): p. 12132-12136.
73. Vega, S.L., et al., *Combinatorial hydrogels with biochemical gradients for screening 3D cellular microenvironments*. *Nat Commun*, 2018. **9**(1): p. 614.
74. Davidson, M.D., et al., *Programmable and contractile materials through cell encapsulation in fibrous hydrogel assemblies*. 2021. **7**(46): p. eabi8157.